FORSCHUNGSZENTRUM KARLSRUHE
in der Helmholtz-Gemeinschaft

Wissenschaftliche Berichte
FZKA 6809

Long-Term Performance of Candidate Materials for HLW/Spent Fuel Disposal Containers

E. Smailos, M.Á. Cuñado[1)], I. Azkarate[2)], B. Kursten[3)], G. Marx[4)]

Institut für Nukleare Entsorgung

[1)] ENRESA, Spain
[2)] INASMET, Spain
[3)] SCK.CEN, Belgium
[4)] GNF.IUT, Germany

EC-Contract No. FIKW-CT-2000-00004

2. Annual Progress Report (November 2001 - October 2002)

Forschungszentrum Karlsruhe GmbH, Karlsruhe
2003

ACKNOWLEDGEMENT

The work was performed within the 5th EURATOM FRAMEWORK PROGRAMME 1998-2002, Key Action: NUCLEAR FISSION.

The authors thank the European Commission in Brussels, Belgium for funding of this project.

Impressum der Print-Ausgabe:

Als Manuskript gedruckt

Forschungszentrum Karlsruhe GmbH
Postfach 3640, 76021 Karlsruhe

Mitglied der Hermann von Helmholtz-Gemeinschaft
Deutscher Forschungszentren (HGF)

ISSN 0947-8620

EXECUTIVE SUMMARY

In the project “Corrosion Evaluation of Metallic Materials for Long-Lived HLW/Spent Fuel Disposal Containers,“ (November 2000 to October 2003) in-depth corrosion studies are performed on preselected container materials in rock salt, granite and clay environments. The materials investigated are carbon steel, stainless steels, Ni-base alloys (Hastelloy C-4 and Hastelloy C-22), the alloy Ti99.8-Pd and Cu-base materials. The objectives of the studies are: to determine the influence of essential parameters (e.g., composition of the medium, temperature etc.) on corrosion, to gain a better understanding of corrosion mechanisms, and to provide more accurate data for modeling the corrosion of the containers over hundred of years. To achieve the objectives of the project, a combination of chemical experiments (long-term immersion tests), electrochemical studies, and stress corrosion cracking studies are performed. The project is a joint undertaken of FZK.INE (project co-ordinator; investigations in rock salt and granite), GNF.IUT (investigations in rock salt), ENRESA/INASMET (studies in granite), and SCK.CEN (studies in clay). In the present paper the results obtained in the second year of the project (November 2001-October 2002) are presented.

The results of long-term immersion experiments on coupled specimens of Ti99.8-Pd and TStE355 carbon steel in $MgCl_2$-rich brine (T=150°C) indicate that in the absence of gamma radiation no contact corrosion occurs. In the presence of gamma radiation of 10 Gy/h, however, severe contact corrosion occurs, which results in a significant increase in the corrosion rate of the steel. Cu and the Cu-Ni alloys 90-10 and 70-30 exhibit in NaCl-rich brine very low corrosion rates (3-12 µm/a). In $MgCl_2$-rich brine the corrosion rates of these materials are clearly higher (24-46 µm/a) than in NaCl-rich brine, and in addition intergranular corrosion was observed on Cu and Cu-Ni 90-10. Electrochemical studies at rest potentials in brines (T=25°C and 80°C) show in agreement with the long-term immersion experiments that the corrosion rates of carbon steel, Cu, Ni, and Cu-Ni alloys in $MgCl_2$-rich brine are higher than in NaCl-rich brine. Contact corrosion studies on material pairs such as carbon steel in contact with Cu, Ni and Cu-Ni alloys or Cu in contact with Ni show that the contact corrosion potential is dominated by the less noble partner, i.e., carbon steel and Cu.

In granitic water with low Cl^- concentration (98 mg/l) at 90°C, the carbon steel is sufficient resistant to pitting corrosion. However, in granitic-bentonite environment with high Cl^- concentration (6280 mg/l), severe pitting corrosion occurs. The results of slow strain rate tests, electrochemical studies, and crevice corrosion experiments (90°C) in granitic-bentonite environments (up to 50000 ppm Cl^-) indicate that the materials Hastelloy C-22, Cu and Cu-Ni 70-30 are resistant to stress corrosion cracking, pitting and crevice corrosion, except the Cu-Ni 70-30 at 50000 ppm Cl-, in which a slight susceptibility to stress corrosion cracking was observed at strain rates of 10^{-6} s^{-1} and $2x10^{-7}s^{-1}$.

In clay water (aerobic conditions, 100-50000 ppm Cl^-, 140°C), the corrosion allowance material TStE355 is subject to general corrosion. Among the passively corroded materials only the alloy Ti99.8-Pd is resistant to pitting and crevice corrosion. The Ni-base alloys Hastelloy C-4 and Hastelloy C-22 show a slight crevice corrosion at Cl^- concentrations higher than 20000 ppm Cl^-. The stainless steels investigated show a lower resistance to pitting corrosion than the Ni-base alloys, but pitting corrosion occurs at Cl^- concentrations which are significantly higher than those expected in the near field environment of the Belgian disposal concept.

KORROSIONSBESTÄNDIGKEIT AUSGEWÄHLTER BEHÄLTERWERKSTOFFE FÜR DIE ENDLAGERUNG VON HOCHRADIOAKTIVEN ABFÄLLEN UND ABGEBRANNTEN BRENNELEMENTEN

ZUSAMMENFASSUNG

Im Rahmen des EU-Projektes „Long-term performance of candidate materials for HLW/Spent fuel disposal containers“ (November 2000-Oktober 2003) wird das Korrosionsverhalten ausgewählter metallischer Werkstoffe unter simulierten Endlagerbedingungen in Steinsalz, Granit und Ton untersucht. Die untersuchten Werkstoffe sind ein unlegierter Stahl, legierte Cr-Ni-Stähle, Nickelbasislegierungen (Hastelloy C4 und Hastelloy C12), die Legierung Ti99,8-Pd und Kupferbasiswerkstoffe (Cu und Cu-Ni-Legierungen). Die Ziele der Untersuchungen sind: Bestimmung des Einflusses wichtiger Parameter auf das Korrosionsverhalten der Werkstoffe, Verbesserung der Kenntnisse über die Korrosionsmechanismen und die Gewinnung von sicheren Daten für ein Korrosionsmodell mit dem die Standzeit der Behälter unter Endlagerbedingungen prognostiziert werden kann. Die Untersuchungen umfassen chemische Experimente (Langzeit-Immersionstests), elektrochemische Untersuchungen und Spannungsrißkorrosionsuntersuchungen. Das Projekt ist ein gemeinsames Vorhaben von FZK.INE (Projektkoordinator, Untersuchungen in Steinsalz und Granit), GNF.INT (Untersuchungen in Steinsalz), ENRESA/INASMET (Untersuchungen in Granit) und SCK.CEN (Untersuchungen in Ton). In der vorliegenden Arbeit wird über die im zweiten Projektjahr gewonnenen Untersuchungsergebnisse berichtet.

Die Ergebnisse der Langzeit-Immersionsexperimente an Kontaktproben aus Ti99,8-Pd und unlegiertem Stahl (TStE355) in $MgCl_2$-reicher Salzlösung (T=150°C) zeigen, daß in Abwesenheit von Gammastrahlung keine Kontaktkorrosion am Werkstoffpaar Ti99,8-Pd/Stahl auftritt. In Gegenwart eines Gammastrahlenfeldes von 10 Gy/h hingegen tritt bei diesem Werkstoffpaar eine starke Kontaktkorrosion auf, die zu einer signifikanten Erhöhung der Korrosionsrate des Stahls gegenüber dem Wert der entsprechenden Einzelstahlproben führt. Die Korrosionsraten von Cu und der Cu-Ni Legierungen 90-10 und 70-30 in NaCl-reicher Lösung (T=150°C) sind sehr niedrig (3-12 µm/a). In $MgCl_2$-reicher Lösung sind die Korrosionsraten dieser Werkstoffe deutlich höher als in NaCl-reicher Lösung (24-46 µm/a) und zusätzlich tritt bei Cu und Cu-Ni 90-10 interkristalline Korrosion auf. Elektrochemische Korrosionsuntersuchungen an Werkstoffpaaren wie unlegierter Stahl in Kontakt mit Cu, Ni und Cu-Ni-Legierungen oder Cu in Kontakt mit Ni (T=25°C und 80°C) zeigen, daß die Kontaktkorrosionspotentiale durch das unedlere Metall Stahl bzw. Cu (im System Cu-Ni) bestimmt wird.

In Granitwasser (T=90°C) mit niedriger Cl^--Konzentration (98 mg/l) zeigt der unlegierte Stahl TStE355 eine ausreichende Beständigkeit gegenüber Lochkorrosion. In Gratitwasser mit hoher Cl^--Konzentration (6280 mg/l) hingegen tritt bei dem Stahl eine starke Lochkorrosion auf. Die Werkstoffe Hastelloy C-22, Cu und Cu-Ni 70-30 sind in Granit-Bentonit Milieu (T=90°C) bis zu 50.000 mg/l Cl^- beständig gegenüber Spannungsrißkorrosion, Lochkorrosion und Spaltkorrosion, ausgenommen der Legierung Cu-Ni 70-30, die bei 50.000 mg/l Cl^- und sehr niedrigen Dehnungsraten von 10^{-6} s^{-1} und 10^{-7} s^{-1} eine leichte Empfindlichkeit gegenüber Spannungsrißkorrosion zeigt.

In Tonwasser (aerobe Bedingungen, 100-50.000 ppm Cl^-, 140°C) sind der Stahl TStE355 und die Legierung Ti99.8-Pd unter allen Prüfbedingungen beständig gegenüber Loch- und Spaltkorrosion. Bei hohen Cl^- Konzentrationen zeigen Hastelloy C-4 und Hastelloy C-22 eine leichte Empfindlichkeit gegenüber Spaltkorrosion und die Cr-Ni-Stähle sind anfällig gegenüber Lochkorrosion. Allerdings sind diese Cl^--Konzentrationen deutlich höher als die im belgischen Endlagerkonzept zu erwartenden Werte.

TABLE OF CONTENTS

1. OBJECTIVES AND EXPECTED OUTCOME

In present concepts for the disposal of vitrified high-level waste (HLW) and spent fuel in geological formations such as rock salt, granite and clay, the disposal container is one of several barriers against the mobilization of radionuclides. The main threat to container integrity is corrosion induced by contact with salt brines or groundwater which may be present in the disposal area under certain conditions. Accordingly, extended studies have been undertaken in various EU-laboratories aimed at identifying corrosion resistant materials for long-lived containers.

Previous corrosion studies in the frame of EC-Projects yielded a considerable amount of information on the corrosion behaviour of various materials such as carbon steel, stainless steels, nickel- and titanium alloys under disposal conditions. A large number of experimental data was gained which could be used for the development of materials degradation models in order to predict the lifetime of the containers. From the results obtained in previous studies [1,2,3,4,5], the following conclusions can be drawn:

- The passively corroded alloy Ti99.8-Pd is the strongest candidate for the corrosion-resistant container concept in rock salt, granite and clay.

- The actively corroded carbon steel is the most promising material for the corrosion allowance container concept in the above-mentioned geological formations. However, its general corrosion rate at high temperature (150°C) in $MgCl_2$-rich brines is very high, which leads to very thick-walled containers and to undesirable high amounts of H_2 in the repository. Therefore, alternative materials such as Cu-base materials will be investigated.

- Hastelloy and high alloyed stainless steels seem to be potential container materials for disposal in clay at realistic Cl^- concentrations.

The objectives of the present corrosion programme are:

- A reliable assessment of the suitability of the above-mentioned candidate container materials in the various repositories by examination of the influence of important parameters on the corrosion behaviour, and clarification of essential questions remaining from the previous EC-project.

- To evaluate the suitability of potential alternative container materials.

- To achieve a better understanding of the corrosion mechanisms and to provide the necessary data for modeling the corrosion of the containers over hundreds of years.

To achieve the objectives of the project, a combination of chemical experiments (long-term immersion tests), electrochemical studies and stress corrosion cracking studies are being performed in the EU-partners´ laboratories.

Essential aspects of the studies in salt environments are to investigate the contact corrosion between Ti99.8-Pd (outer container) and carbon steel (inner container) and to examine the influence of welding (simulation of a container closure technique) and thermal stress relief treatment of the welds on the corrosion behaviour of carbon steel.

Further important points are the evaluation of copper and copper alloys as container materials (alternative materials for carbon steel) and the examination of the influence of gamma radiation on the corrosion of the various materials. In granitic environment, the corrosion behaviour of various materials (steel, copper-base, and nickel-base materials) to general and local corrosion and stress corrosion cracking will be investigated. In clay/bentonite environment, the influence of various parameters (anaerobic conditions, elevated temperature and radiolysis products) on the corrosion of carbon steel, stainless steels, Hastelloy C4 and C22, and Ti99.8-Pd will be studied.

The corrosion results can be used to develop materials degradation models in order to predict the lifetime of the containers over hundred of years. A container corrosion model can be combined with other models (e.g. spent fuel and HLW glass models) to describe the source term in the near field in the framework of safety analyses for a repository.

The results will be disseminated to organizations responsible for implementing the programmes for disposal of radioactive waste and will be published in accordance with the rules set up by the European Commission. Since all partners are involved in research into repository safety, the participating organizations will be also end-users of the results.

The results of the project could be used in all European Union countries as the project is independent of the type of fuel cycle of HLW waste (spent fuel or glass) and the characteristics of the host rock environment.

In the present report, the progress achieved in the research programme from November 2001 to October 2002 shall be described.

2. SCIENTIFIC AND TECHNICAL PERFORMANCE

2.1 Corrosion studies in salt environments (WP1) (FZK.INE, GNF.IUT)

2.1.1 Contact corrosion between Ti99.8-Pd and carbon steel in $MgCl_2$-rich brine (WP1.2) (FZK.INE)

A potential packaging design for vitrified HLW and spent fuel is the use of a double-walled container (overpack) surrounding the canisters. This consists of an inner thick-walled carbon steel container as mechanical support against the rock pressure which is corrosion protected by a thin-walled container made of the alloy Ti99.8-Pd. By attack of salt brine and penetration of the outer Ti99.8-Pd container (e.g. by pitting corrosion), a direct contact can be established between the brine and the two different container materials. In this case, a contact corrosion potential will be formed. If the contact potential is high enough, a significant increase in the corrosion rate of the less noble carbon steel and a decrease in the corrosion rate of the more noble Ti99.8-Pd is expected. Nevertheless, in many cases the contact corrosion is negligible low so that the corrosion rate of the individual materials will not be

changed. This is the case for passive corroding materials. Under this aspect it is investigated in this study if by attack of $MgCl_2$-rich brine, a significant contact corrosion occurs on the metal pair Ti99.8-Pd and TStE355 carbon steel. Corresponding contact corrosion studies in NaCl-rich brine were performed in previous work [6].

Experimental

The materials TStE355 carbon steel and Ti99.8-Pd were investigated in the hot-rolled and annealed condition and had the following composition in wt.%:

- TStE355 steel: 0.17 % C; 0.44 % Si; 1.49 % Mn; bal. Fe.
- Ti99.8: 0.18 % Pd; 0.05 % Fe; 0.01 % C; 0.04 % O_2; bal. Ti.

Contact assemblies were formed by bolting one flat coupon of Ti99.8-Pd (40 mm x 20 mm x 4 mm) with one flat coupon of carbon steel (40mm x 20mm x 4mm). The two coupons were provided with bores in both ends and were fastened with titanium screws. The bores were isolated by PTFE. With this specimens type, the metals were joined very tight.

The long-term corrosion behaviour of the materials was investigated in the disposal relevant $MgCl_2$-rich Q-brine. The brine had the following composition at 55°C (wt.%):

Q-brine: 26.8 $MgCl_2$; 4.7 KCl; 1.4 NaCl; 1.4 $MgSO_4$; 65.7 H_2O (pH=4.6)

The experiments lasted up to about 18 months and were performed at a temperature of 150°C, which roughly corresponds to the maximum surface temperature of the container according to the disposal concept discussed in Germany. Experiments were performed both with and without gamma radiation of 10 Gy/h. This dose rate corresponds to the value on the surface of a thick-walled disposal container discussed having mechanical and corrosion allowances of about 100 mm for a lifetime of 300 years.

Experiments under gamma radiation are important because the interaction of gamma radiation exerted by the waste with brines produces reducing/oxidizing reactive particles and stable products (e.g., H_2, O_2, ClO_3^-) which may change the rate and mechanism of corrosion. Furthermore, the absorption of gamma radiation in passive oxide layers of metals (e.g. Ti) will induce photoradiation effects, which may change the corrosion rate.

The experimental setups used for the experiments are described in previous work [5] Briefly, for the experiments without irradiation, stainless steel pressure vessels provided with corrosion resistant insert vessels made of PTFE were used to avoid evaporation of the brine (boiling point: about 115°C). The experiments under gamma irradiation were performed in the spent fuel storage pool of FZJ Jülich. For these experiments, autoclaves made of Ti99.8-Pd were used. Every autoclave contained 160 ml brine and two coupled specimens of 80 cm^2 total surface. This gave a brine volume-to-specimen surface ratio of 2 ml/cm^2. With these experimental equipments, the initial test conditions were oxidizing. The initial total amount of the oxygen available in the systems was about 15 mg, corresponding to 0.19 mg O_2/cm^2

specimen. This oxygen amount was consumed very fast by reactions with Fe so that after a few days reducing conditions were established.

Evaluation of the specimens regarding general and local corrosion was carried out by gravimetry, measurements of pit depth, surface profilometry and metallography. Both the contact area and the free specimen area were investigated for local corrosion attacks. The integral corrosion rate of the specimens was calculated from the experimental determined weight losses and the material density.

Results

The time-dependence of the integral thickness reduction (general corrosion) of the coupled specimens of Ti99.8-Pd and TStE355 carbon steel at 150°C in Q-brine with and without a gamma radiation field is plotted in Figures 1 and 2. The data indicate that the thickness reduction of Ti99.8-Pd in the brine both with and without radiation (0.2 µm at the maximum) is only a little higher than the detection limit (0.01 µm). This is attributed to the formation of a very stable passive oxide surface film consisting of TiO_2.

The thickness reduction of the steel in the brine without irradiation (Figure 1) remains during the test time between 147 days and 340 days fairly constant, which means that the corrosion rate decreases with time. This is due to the formation of a protective corrosion layer on the specimens surface consisting of (Fe, Mg)$(OH)_2$. However, after longer test duration than 340 days, the corrosion layer was locally penetrated which resulted to an increase of the corrosion rate. In Q-brine and in the presence of gamma radiation (Figure 2), the thickness reduction of the specimens increases linearly over the whole test duration and is significantly higher (about 320 µm after 310 days) than the value without irradiation. In addition, very deep local corrosion was observed on the steel specimens exposed to irradiated brine.

The calculated integral corrosion rates of the coupled specimens of Ti99.8-Pd and carbon steel in Q-brine at 150°C with and without gamma radiation are compiled in Table 1. For comparison, the values of uncoupled (single) specimens of these materials determined in previous investigations [3,5] are also given in the Table. For Ti99.8-Pd, the corrosion rates of the coupled specimens both with and without gamma radiation are negligible low (0.08 µm/a – 0.2 µm/a) and very close to the values of the uncoupled specimens (0.02 µm/a – 0.2 µm/a). Also for the carbon steel, the corrosion rate of the coupled specimens in the absence of radiation (36.6 µm/a ± 14.5 µm/a) corresponds well to the value of the unirradiated uncoupled specimens (47.1 µm/a ± 2.5 µm/a). This indicates that the solid corrosion product (Fe, Mg)$(OH)_2$ can sufficiently protect the actively corroded steel against contact corrosion, and that the contact corrosion potential lies apparently near to the rest corrosion potential of the steel. The small differences between the corrosion rates found for Ti99.8-Pd and carbon steel in the brine are in the range of the standard deviation of the values. In the Q-brine and in the presence of gamma radiation , however, the corrosion rate of the coupled steel specimens (369 µm/a) increases significantly, compared to that without radiation (36.6 µm/a ± 14.5 µm/a) and is by a factor of about 5 higher than the value of the irradiated uncoupled specimens (72.6 µm/a ± 11 µm/a). A possible explanation for the strong increase of the corrosion rate of the coupled steel specimens in irradiated Q-brine is that the oxidants, mainly O_2, formed by the

radiolysis of water are reduced at the Ti99.8-Pd cathode, which results to an increase of the oxidation rate of Fe analog to a local element.

The metallographic examinations of coupled Ti99.8-Pd specimens exposed to irradiated and unirradiated Q-brine do not show any signs of local corrosion neither in the contact area to the steel nor in the free specimen area. For all Ti99.8-Pd specimens a completely uniform corrosion was observed. The coupled steel specimens corroded in the Q-brine without irradiation non-uniformly, but the maximum depth of this uneven general corrosion was only about 70 µm after 538 days. In the presence of gamma radiation, however, the coupled steel specimens suffered from very strong local corrosion in the brine. The maximum local corrosion depth after 538 days exposure to the irradiated Q-brine was about 500 µm. This explains the high average general corrosion rate of the steel in the irradiated brine environment.

2.1.2 Corrosion behaviour of copper-base materials in salt brines (WP1.3) (FZK.INE)

In previous corrosion studies in salt brine environments [3,4,5], the passively corroded alloy Ti99.8-Pd and the actively corroded carbon steels („corrosion-allowance“ materials) were identified as candidates for a container corrosion barrier. In the event that these materials prove inadequate as a corrosion barrier, Cu-base alloys are investigated as alternate container materials. In the present work, the suitability of three Cu-base materials (Cu, Cu-Ni 90-10 and Cu-Ni 70-30) as corrosion barrier materials was examined. For this, the long-term corrosion behaviour of the materials was investigated in two disposal relevant brines by using immersion tests.

Materials and experimental

The Cu-base materials were investigated in the brines in the hot-rolled and annealed condition and had the following composition in wt.%:

Cu: 99.9995 Cu; O: 0.0005
Cu-Ni 90-10: 88.5 Cu; 9.9 Ni; 1.3 Fe; Rest: C, Mn, P, S
Cu-Ni 70-30: 69.3 Cu; 29.3 Ni; 0.6 Fe; Rest: C, Mn, P, S

For the experiments plane specimens having the dimensions 40mmx20mmx4mm were used.

The corrosion media were two disposal relevant brines. One of them was NaCl-rich, the other one $MgCl_2$-rich. The brines had the following composition in wt.%:

NaCl-rich brine: 25.9 NaCl; 0.23 K_2SO_4; 0.21 $CaSO_4$; 0.16 $MgSO_4$; 73.5 H_2O (pH(25°C)=6.5).
$MgCl_2$-rich brine (Q-brine): 26.8 $MgCl_2$; 4.7 KCl; 1.4 NaCl; 65.7 H_2O; (pH(25°C)=4.6).

The materials were investigated in the brines for up to 15 month at the temperature of 150°C. In order to get information on the influence of gamma radiation on the corrosion behaviour of the materials, additionally experiments were performed in the NaCl-rich brine in the presence of a gamma radiation field of 10 Gy/h. The

experimental setups and the method used for the corrosion evaluation of the materials are discribet in section 2.1.1.

Results

Figures 3-5 show the time-dependence of the general corrosion, expressed as the integral thickness reduction of the three Cu-base materials in the brines at 150°C. The data indicate that the general corrosion of the specimens both with and without gamma radiation increases linearly with the exposure time in the brines over the test duration of this study. The linear corrosion rates of the materials in the brines were calculated from the slope of the curves and are compiled in Tables 2 and 3.

In the NaCl-rich brine (Table 2) the corrosion rates of the materials are very low (3-12 µm/a), and the imposition of a 10 Gy/h gamma radiation field does not increase the corrosion rate of the materials in this brine. In fact, the corrosion rates under gamma radiation (0.4-1.3 µm/a) are lower than those without irradiation. This is attributed to the formation of more dense Fe_3O_4-corrosion protective surface layers than in the unirradiated brine, as was observed in the metallographic examinations. In the $MgCl_2$-rich Q-brine (Table 3) the corrosion rates of the Cu-base materials amount 24-46 µm/a and are clearly higher than in the NaCl-rich brine. The higher corrosivity of the $MgCl_2$-rich brine compared to the NaCl-rich brine is attributed to its higher HCl concentration. This could be explained by the higher Cl^- concentration and the hydrolysis of Mg^{2+}.

It is evident from the surface profiles and the metallographic examinations of corroded specimens that all three Cu-base materials investigated are resistant to pitting corrosion in the brines in the sense of an active-passive corrosion element. In NaCl-rich brine, the materials corrode uniformly. In the $MgCl_2$-rich Q-brine, the materials were subject to non-uniform general corrosion. In addition, in this brine intergranular corrosion was observed on Cu and the alloy Cu-Ni 90-10. However, the maximum penetration depth of the non-uniform corrosion corresponds to the values of the average thickness reduction of the specimens and the intergranular corrosion after 15 months was only about 100 µm at the maximum.

2.1.3 Electrochemical studies on copper, nickel, copper-nickel alloys and carbon steel (WP1.3) (GNF.IUT)

GNF/IUT investigates the corrosion behaviour of Cu, Ni, Cu-Ni-90-10, Cu-Ni 70-30 and TStE355 carbon steel (0.17 wt.% C) in brines ($MgCl_2$-rich Q-brine and NaCl-rich brine 3) at 25°C and 80°C by use of electrochemical and analytical methods. In the reporting period GNF/IUT work focused on the following topics:

- Completion of the measurements of the rest potentials of Cu, Ni, Cu-Ni-alloys 90-10 and 70-30 and carbon steel in the $MgCl_2$-rich Q-brine (26.8 wt% $MgCl_2$) and in NaCl-rich brine (25.9 wt% NaCl) at 25°C and determination of the corrosion rates.

- Performance of corrosion experiments on the materials aforementioned in Q-brine and NaCl-rich at the higher temperature of 80°C.

- Determination of the contact potentials and the corrosion rates of the above-mentioned materials in brines at 25°C and 80°C.
- Examination of analytical problems by applying ICP-MS (Induced Coupled Plasma Mass Spectroscopy), RiM (Radio isotope Method) and the classical weighting method.

- Comparison of TXRF with ICP/MS with respect to their application to the experiments performed.

Experimental

Potentiodynamic and potentiostatic measurements were carried out on the materials mentioned above in the relevant brines at two different temperatures (25°C; 80°C). The corrosion rates were mostly determined analytically from weight loss. But also TXRF and especially ICP/MS were applied, on condition that the necessary parameters of these methods could be realized.

Results from the measurements at rest potentials in brines at 25°C and 80°C

The rest potentials and the corrosion rates of the various materials at 25°C are compiled in Table 4. The data indicate that in both brines (Q-brine and NaCl-rich brine) the corrosion rates of Ni are smaller than of Cu. The corrosion rates of Cu are slightly higher in Q-brine than in NaCl-brine. Furthermore, the corrosion rate of carbon steel is also higher in Q-brine than in NaCl-rich brine, and can be compared with the data obtained for Cu. Moreover, it can be outlined that the corrosion rates of the Cu-Ni-alloys are higher in Q-brine than in NaCl-rich brine. Comparing the corrosion rates of Cu-Ni 90-10 with those of Cu-Ni 70-30 it can be stated that the corrosion rates of the alloy with the higher Cu content are higher and nearly identical with those of carbon steel in the relevant brine systems. Winding up the results it can be shown that at 25°C, an increasing Ni content of the alloys increases the resistance of the material to corrosion in brines under the experimental conditions applied in these studies.

At the higher test temperature of 80°C (c.f. Table 5), the corrosion rates of the materials investigated are significantly higher than those obtained at 25°C in the identical media. Moreover, it can be shown, that the relevant corrosion rates are higher in Q-brine than in NaCl-solution, except those for Ni. This phenomenom could be explained by the fact that Ni forms two passive ranges [7], the first one being due to the formation of a NiO layer, the second one to a NiO(OH) layer. At higher temperatures NiO(OH) is transformed into $Ni^{(II)}Ni^{(III)}{}_2O_2(OH)_4$, which might deliver the resistant $MgNi^{(III)}{}_2O_4$ spinell, if sufficient Mg^{2+} is present, as is the case for Q-brine. On the other hand it must be taken into account that $Ni^{(III)}$ spinells are unknown, also the compound Ni_3O_4, which should be an analogon to the spinells Co_3O_4 and Fe_3O_4. Furthermore there exist $Sr_2Ni^{(III)}{}_2O_5$ and $Ca_2Ni^{(III)}{}_2O_5$ [8] Therefore, the determination of the structure of the oxide layer of Ni is urgently needed, in order to find out, which chemical compound is responsible for the relativ high resistance of Ni towards corrosion in Q-brine. The relative higher corrosion of the investigated materials in Q-brine compared with that in NaCl-rich brine can be explained by the lower pH value of Q-brine due to the hydrolysis of $MgCl_2$. This effect is even greater at higher

temperature, because the hydrolysis constant depends on temperature in form of an e-function (Vant' Hoff).
In general, the increase of corrosion by rising temperature can also be understood from the dependence of the corrosion current I_{corr} on the temperature, which is described by the well known modified Stern - Geary equation

$$I_{corr} = b_a \cdot b_c / (b_a + b_c)\, R_p \equiv B \cdot 1 / R_p \qquad (1)$$

with $b_a = R \cdot T / \alpha_a \cdot z_a \cdot F$ and $b_c = R \cdot T / \alpha_c \cdot z_c \cdot F$ (1a)

In this equation Rp is the polarization resistance; R the universal gas constant, F the Faraday constant, T the absolute temperature, z_a and z_c the number of electrons exchanged at anode and cathode respectivly by the redox reaction and α_a and α_c the relevant transfer coefficients.

The first diviation of (1) leads to (2)

$$d\, I_{corr} / dT = dB / dt \cdot 1 / R_p = R / F \cdot 1 / \alpha_a \cdot z_a + (1 - \alpha_c)\, |z_c| \cdot 1 / R_p$$

on condition, that R_p is constant.

In case of $\alpha_a = \alpha_c = 0{,}5$ and $z_a = |z_c| = 1$ it follows:

$$DB / dT = 0{,}08\ mV \times K^{-1}$$

Comparing the corrosion rates of the materials obtained at rest potential at higher temperature (80°C) with each other it can be outlined that in contradiction to the relevant results obtained at 25°C, Cu is more resistant towards corrosion than Ni, whereby the lowest corrosion rate exhibits the alloy Cu-Ni 90-10 in Q-brine. To clarify the reason for this behaviour, the relevant formed oxide surface layers must be studied in detail.

Results from the measurements at contact potentials at 25°C and 80°C

The contact corrosion potentials and the corrosion rates of the various materials determined at 25°C and 80°C in the brines are compiled in Table 6. The data indicate that the contact potential is dominated by the more negative partner, which is the carbon steel, whenever this material is combined with Ni or Cu or their alloys. In case of a contact between Ni and Cu , Cu is the more negative partner and dominates the contact potential. The contact potential nearly equals the rest potential of the negative partner, but due to the positive slope of the Butler-Volmer-equation its corrosion rate is significantly increased. The corrosion rate of the positive partner on the other hand ist decreased in accordance with the theory. Carbon steel or Cu acts as cathode protector respectively.

At 80°C the corrosion rates of both contact partners are drastically higher, except the Cu-Ni alloys, this phenomenom being due to the dependence of the equilibrium potential and the rest potential on temperature. Since the Butler-Volmer-equation ist only specific for each system at a certain temperature, comparing the relevant potentials with each other has to be done very carefully. From the Figures 6 and 7 it can be seen, that it takes approximately 95 h until constant experimental conditions are reached for contact corrosion measurements. Winding up the results it can be demonstrated (see Table 6) that under the applied conditions at both test temperatures, Ni is the more resistant material towards corrosion in all the relevant systems, in which contact corrosion was measured.

Analytical problems by applying ICP-MS, RiM and the classical weigh loss method

ICP-MS (Induced Coupled Plasma Mass Spectroskopy) and RiM (Radio isotope Method) are methods which determine only the amount of corroded material, which ist dissolved in the test solution. Therefore, precipitated material or material still adhering to the electrode must be totally dissolved after the end of the experiment. Otherwise wrong results will be obtained. Table 7 shows a comparison of the corrosion rates of the materials at rest potential at 80°C obtained from surface treated and untreated electrodes, whereby the values obtained from the untreated electrodes are the wrong ones. In general, total dissolution of the material can be achieved by acidifying the solution. Applying the classical weighing method on the other hand, the material adhering to the electrode must always be removed before weighing in order to get a cleaned electrode for this analytical operation.

Comparison of TXRF with ICP-MS for analyses of corrosion products

TXRF (Total Reflection X-ray Fluorescence) is a very sensitive method for trace analysis due to its small signal-noise ratio, which is caused by the very small amount of scattered X-rays. It can be seen from Figure 8 that the matrix influence of Q-brine on the results cannot be neglected. A dilution factor of at least 50 is necessary to obtain accurate results when using TXRF as an analytical tool for Cu and Ni determinations. The same is true also for the NaCl-rich brine 3. The TXRF spectra, which are to be seen in Figure 9 demonstrate optically the necessity to dilute the samples to a sufficient amount. Since elements with small atomic numbers have a greater signal depression, Ga must be chosen as an inner standard instead of Mn, which was selected before. This investigations show up very clearly the limits of TXRF as an analytical method for corrosion experiments. Due to the high dilution of the solution being necessary to apply this method its sensitivity is to low for analyzing traces of the corrosion products. The difference of sensitivity of ICP-MS with respect to TXRF is 2 to 3 decades. Therefore, the first one has to be preferred as an analytical tool to study corrosion.

2.2 Corrosion studies in granitic environments (WP2) (FZK.INE, ENRESA-INASMET)

2.2.1 Long-term immersion studies on carbon steel (WP2.1) (FZK.INE)

The long-term corrosion behaviour of the preselected TStE355 carbon steel was investigated in two disposal relevant granitic environments by using immersion

experiments. The steel was examined in the hot-rolled and annealed condition and had the following composition in wt.%:
0.17% C, 0.44% Si, 1.49% Mn, bal. Fe.

For the investigations, flat specimens having the dimensions 40 mm by 20 mm by 4 mm were used.

In order to examine the influence of the Cl^- content of granitic water on the steel corrosion, two synthetic granitic waters having different Cl^- contents were selected as corrosion media. These were: a granitic water with a low Cl^- content of 98 mg/l (granitic water 1) and a granitic water which was in contact with bentonite and had a very high Cl^- content of 6260 mg/l (granitic water 2). The compositions of the granitic waters are given in Tables 8 and 9.

The specimens were investigated in the granitic waters for up to 15 months at a temperature of 90°C which corresponds to the maximum surface temperature of the containers according to the disposal concepts in a granitic formation. For the experiments, stainless steels pressure vessels with corrosion-resistant polytetrafluorethylene (PTFE) inserts of 210 ml volume were used to avoid evaporation of the granitic waters at the test temperature. Each PTFE insert contained 160 ml of corrosion medium and four specimens of 80 cm^2 total surface. The specimens were suspended by PTFE threads, which were fixed below the lid of the insert. After tightly closing the inserts, the vessels were stored in heated chambers at the test temperature of 90°C.

With these experimental equipment, the initial test conditions were oxidizing. The total amount of oxygen available in the system was about 16 mg, corresponding to 0.2 mg O_2/cm^2 specimen. It consisted of the oxygen content in the 50 ml of air space (15 mg O_2) above the granitic water and the dissolved oxygen (1 mg) in the 160 ml of granitic water. The latter was measured in the autoclaves before starting the experiments by a polarographic method using an O_2 sensor. The value determined at 25°C (6 mg of O_2/l) corresponds to the saturation value in air obtained by the Winkler method. This oxygen amount was consumed by reactions with Fe so that after a few days reducing conditions were established. Evaluation of the specimens regarding general and local corrosion was carried out by gravimetry, measurements of pit depth, surface profilometry and metallography.

Results

The general corrosion of the TStE355 carbon steel in the granitic waters 1 and 2 was determined from the weight losses of the specimens and the material density. Figures 10 and 11 show the time-dependence of the general corrosion of the steel, expressed as the integral thickness reduction of the specimens, in the granitic waters at 90°C. The data indicate that the general corrosion of the steel in both test media increases linearly with the exposure time over the test duration of the study. The linear corrosion rates of the steel in the granitic waters, calculated from the slope of the curve, and the results of the local corrosion determined by surface profilometry and metallography are compiled in Table 10.

It is evident from Table 10 that the linear corrosion rate of the TStE355 carbon steel in both granitic waters is low (21.1µm/a and 22.6 µm/a, respectively). The reason for the small general corrosion rates of the steel in both corrosion media is the formation of a tight protecting corrosion layer on the specimens surface. This black corrosion layer was identified by X-Ray Diffraction (XRD) analysis as Fe_3O_4 (magnetite). However, in the granitic water with a high Cl^- concentration of 6260 mg/l (granitic water 2) the corrosion surface layer broke down locally, resulting to severe pitting corrosion with a maximum depth of up to 1200 µm after 300 days test duration. On the contrary, in the granitic water with a low Cl^- concentration of 98 mg/l (granitic water 1), a very few small pits of about only 60 µm at the maximum were detected after 300 days exposure to the medium.

The results of Fe-analyses of solution samples and solid samples (sediments and corrosion products remaining on the steel specimens` surface) taken from granitic water with high Cl^- concentration (6260 mg/l) are summarized in Table 11. The solution samples were analyzed for $Fe_{(tot)}$ by ICP/AES, for Fe^{2+} and Fe^{3+} by Ion Chromatography (IC). The solid samples were analyzed for Fe^{2+} and Fe^{3+} after chemical dissolution in HCl. The results indicate that Fe is present in the granitic water only in a very small amount, probably in colloidal form. In the solid corrosion products taking from the specimens` surface and from the bottom of the vessels, high amounts of Fe^{2+} and Fe^{3+} were determined, whereas especially in the corrosion products on the bottom of the vessels the amount of Fe^{3+} is higher than that of Fe^{2+}.

On the base of the results obtained in this study it can be stated that the TStE355 carbon steel is a potential HLW container material only for granitic formations in which the groundwater has a low Cl^- content. Furthermore, it can be stated that the corrosion behaviour of the steel in granitic environments with high Cl^- content is different as that in high concentrated salt brines, in which only non-uniform corrosion and not pitting corrosion was obtained [4].

2.2.2 Localized corrosion studies (WP 2.2 and WP 2.3) (ENRESA/INASMET)

The objective of this work is to evaluate the susceptibility of three candidate waste package container materials to certain types of localized corrosion such as stress corrosion cracking (SCC), pitting and crevice corrosion in granitic-bentonite environments. The studied materials are the higher corrosion resistant nickel base material Hastelloy C-22 (UNS N06022) and the intermediate corrosion resistant Cu-OF (UNS C10200) and Cu30Ni (Cu-Ni70-30, UNS C71500) cupronickel alloy. Slow Strain Rate Tests (SSRT), electrochemical and crevice corrosion tests are performed in order to assess the corrosion behaviour of the proposed alloys.

Work performed during this period has been focused on SSR tests, crevice and potentiodynamic polarization tests for the parent and welded specimens.

Materials and corrosion environment

The chemical composition of the studied materials is given in Table 12. Besides the parent metal, Electron Beam (EB) and Gas Tungsten Arc (GTA) welding procedures are also considered in this study for the three candidate materials.

Chemical analysis of the synthetic granitic-bentonite water is given in Table 13 [9]. In order to investigate the effect of chlorides in the corrosion resistance of the selected alloys, different chloride concentrations ranging from 6500 to 50000 ppm Cl^- were used. The investigations were performed at 90ºC, except for the electrochemical corrosion studies in which in addition to 90°C experiments studies were carried out also at 25°C in order to evaluate the effect of lower temperature.

Stress corrosion cracking studies

The susceptibility to SCC was studied by means of the Slow Strain Rate Technique (SSRT). A tensile specimen in contact with a specific environment is continuously strained in tension until fracture. The tests were conducted according to the requirements described in ISO 7539-7 [10] and ASTM G 129 [11]. The specimens were tested in granitic-bentonite water and in argon as inert reference medium at 90ºC and strain rates ranging from 10^{-5} to $2x10^{-7}$ s^{-1}. Such strain rates are considered as the most suitable for testing of steels, copper and nickel alloys. After each test, the elongation, reduction of area, maximum load, true stress at fracture and time to fracture are measured in order to assess the loss of ductility of the studied materials. This was complemented by metallographic studies performed by optical microscopy in order to identificate secondary cracks, and fractographic analysis, with the aim of evaluating the morphology of cracking. Secondary cracks and failure mode are indicatives of susceptibility to stress corrosion.

Results of stress corrosion cracking studies

HC-22

No loss of ductility or mechanical strength was noticed for HC-22 specimens when tested in the granitic environments with respect to the results obtained in argon. No secondary cracks were observed in the metallographic analysis. Fracture surface examinations show totally ductile fracture surfaces, with dimples formation, for specimens tested in argon and in the granitic water, even at the highest chloride content (50000 ppm).

Similar results are obtained for EB and GTA welded specimens. No secondary cracking is observed at any of the testing conditions (Figure 12), which indicates that the welding procedure has no influence on the resistance of the HC-22 alloy to stress corrosion cracking (SCC).

Cu-30Ni

A summary of the results obtained in the slow strain rate tests on the Cu30Ni alloy are given in Table 14. Compared to the values in argon, no loss of ductility is noticed for the cupronickel alloy when tested in the granitic environments. However, the metallographic studies (Figure 13) reveal secondary cracks when tested in granitic water with the highest chloride content of 50000 ppm at strain rates of 10^{-6} and $2x10^{-7}s^{-1}$, which indicates a slight sensitivity to SCC under the test conditions applied. At 50000 ppm chloride, the deepest secondary crack measured on longitudinal sections of the gage length is 120 microns. When testing at 6500 ppm chloride, the maximum crack depth is 80 microns. For the two above-mentioned strain rates, the crack

density and the maximum crack length values are similar. Fractographic examinations of tested specimens show in general a ductile failure mode. For those specimens tested in the granitic water with 50000 ppm, small brittle intergranular areas in the fracture surface border were observed (Figure 14).

Tests carried out with welded Cu30Ni specimens, reveal also a slight secondary cracking in the base material, when tested in the granitic water with a chloride content of 50000 ppm at strain rates of $10^{-6}s^{-1}$ and $2x10^{-7}s^{-1}$. The maximum crack length values are similar to those obtained for unwelded specimens.

Cu-OF

The values of reduction of area obtained in the slow strain rate tests are shown in Figure 15. It can be stated that the values obtained in the granitic environments are very close to those obtained in argon, which indicates that these granitic environments have no effect on the ductility behaviour of the Cu-OF specimens. The significant drop in the reduction of the area values with decreasing strain rate in both environments is due to a hardening straining phenomenum, and not to environmental conditions. In general, the low values of ductility obtained for copper are attributed to metallurgical parameters such as grain size and degree of work hardening. No secondary cracks were noticed in the metallographic studies at any of the testing conditions (Figure 16). Investigations on Cu-OF welded specimens are in progress.

Electrochemical corrosion studies

Information on the corrosion rate, pitting susceptibility and passivity of the studied materials was obtained by using the potentiodynamic polarization technique. The potentiodynamic tests were conducted according to ASTM G-59 standard [12] and ISO/CD 17475 Test Method [13], in a electrochemical glass cell which contained both the metal to be investigated and the environment in which the polarization scan was going to be performed. This cell has ports through which the working electrode (test specimen), the platinum counter and a salt bridge connected to a Saturated Calomel reference Electrode (SCE) are inserted. An external heater was used to maintain the desired temperature. During the test, N_2 was continuously bubbled into the solution through a fritted glass tube in order to create a deaerated solution. Test specimens measuring 15 mm in diameter and 2 mm thickness, with a 600 grit finish, were mounted in a Teflon holder, leaving an area of $1cm^2$. Tests were performed in the simulated granitic water containing 6500, 15000 and 50000 ppm of chloride at two different temperatures, namely 25°C and 90ºC.

To control the potential and to measure the current, a potentiostat was used. Prior to the start of each test the E_{corr} of the specimen was measured. The potential scan started from a potential -200 mV below E_{corr} and was increased at a rate of 0,167 mV/s. Once the current density reached a value of 10 mA/cm^2 or 2V, the direction of the potential scan was reversed at the same scan rate. The results were plotted as a polarization curve of potential (V) vs. current density (Amp/cm^2). From this curve, the corrosion potential E_{corr}, the pitting potential E_{pit} and the general corrosion rate, can be obtained. The uniform corrosion rate was calculated according to specifications provided in ASTM G-102 [14].

Results of electrochemical studies

The corrosion data obtained from the polarization curves of the three alloys in the granitic environment at 90ºC are summarized in Table 15. No susceptibility to pitting in chloride contents up to 50000 ppm was detected for the three alloys both in the parent and in the welded condition. Polarization curves obtained in the potentiodynamic tests for the Cu30Ni and HC-22 alloys, respectively, in their parent and welded state are given in Figures 17 and 18. Optical examinations of tested specimens (Figure 19) confirm the absence of pits at any testing conditions. Specimens with welded joints have been chemically etched in order to reveal the welded joint, the HAZ (heat affected zone) and the parent base material.

For copper alloys, the increase of chloride concentration increases the general corrosion rate. It should be noted that in the case of passivation of the material or occurrence of pitting or other type of localized corrosion, the calculation of the corrosion rate according ASTM G-102 is not representative. Calculation of uniform corrosion rates from electrochemical tests is useful in the case of materials with general corrosion behaviour, such as carbon steels and some copper alloys. Investigations on Cu-OF welded specimens are in progress.

Crevice corrosion studies

Crevice assemblies were formed by bolting together flat test specimens with crevice formers made of Teflon, according to ASTM specifications G-78 [15]. The resulting assemblies were immersed in autoclaves containing the granitic-bentonite solution with different chloride contents ranging from 6500 to 50000 ppm. The tests were conducted at 90ºC and the test duration was 1, 6 and 12 months. Welded and base materials were evaluated. The specimens were weighed before and after testing in order to determine the corrosion rates of the copper alloys.

Results of crevice corrosion studies

The analysis performed on tested specimens indicate no crevice attack for the three alloys when tested up to 12 months in the granitic-bentonite water at 90ºC and chloride contents up to 50000 ppm.

After testing, the HC-22 specimens show the same appearance as before the testing. The Cu30Ni and Cu-OF alloy specimens show general corrosion in the specimen areas exposed to corrosion media, but no localized attack is observed in areas contacting the teflon crevice formers (Figure 20).

Crevice corrosion tests of welded specimens are currently undergoing**.**

2.3 Corrosion studies in clay environments (WP3) (SCK.CEN)

The aim of the investigations is to evaluate the influence of the oxygen content (work package 3.1), elevated temperature (work package 3.2), and radiolytic products (work package 3.3) on the localized corrosion behaviour of preselected candidate container materials in clay environments.

In the reporting time, work has been concentrated on the evaluation of the influence of elevated temperature on the susceptibility of various preselected container materials to pitting corrosion in Synthetical Oxidizing Claywater solutions (SOCW). Such solutions simulate the near-field environment of an underground repository constructed in a deep geological Boom clay formation. The experiments were performed in autoclaves at 140°C under aerobic conditions. These conditions simulate the disposal period immediate after closure of the underground repository (high temperature and presence of oxygen), in case that the excavated Boom clay is re-used as backfill material. In these experiments, the influence of the content of various anions (chloride, sulphate, and thiosulphate) on the susceptibility of the materials to pitting corrosion was investigated.

The susceptibility to pitting corrosion was determinded by performing Cyclic Potentiodynamic Polarization (CPP) measurements. The long-term corrosion behaviour of the materials was established by comparing the data from the CPP-measurements (the pit nucleation potential, E_{NP}, and the protection potential, E_{PP}) with the actual corrosion potential, E_{CORR}, which was determined by monitoring the Open Circuit Potential (OCP) as a function of time over a period of about 3 months. In Boom clay and under aerobic conditions, E_{CORR} was measured to be +320 mV_{SHE} This value is indicated on all graphs as a horizontal dotted line for easier interpretation of the results.

2.3.1 Materials and experimental techniques

Materials

The susceptibility of eight candidate container materials to localized corrosion was evaluated. These are: carbon steel TStE 355, stainless steels AISI 316L, AISI 316Ti, AISI 316L hMo and UHB 904L, nickel alloys Hastelloy C-4 and Hastelloy C-22, and the titanium alloy Ti/0.2Pd (Ti99.8-Pd,TiGr-7). The chemical composition of these materials is given in Table 16.

Electrochemical techniques and setup

The experimental approach via electrochemical testing is twofold:

- on the one hand, cyclic potentiodynamic polarization (CPP) measurements are performed to provide three characteristic potentials: (i) E_{NP}, the critical pit nucleation potential or breakdown potential (i.e. the potential above which new pits nucleate and grow), (ii) E_{PP}, the protection potential or repassivation potential (*i.e.* the potential above which existing pits can grow, but new pits cannot nucleate; beneath this potential, pits do neither grow nor nucleate), and (iii) OCP, open circuit potential (*i.e.* the potential that the metal assumes in the studied electrolyte under open circuit conditions). The protection potential is derived in two alternative ways: (i) E_{PP1}, the potential where the reverse scan intersects the forward scan or (ii) E_{PP2}, the potential, on the reverse scan, where the current density becomes zero, i.e. where the anodic current is equal to the cathodic current. The CPP technique was chosen because it provides a reasonable, rapid

method for predicting the tendency of an alloy to suffer localized corrosion in the form of pitting. The CPP-curves were recorded with a scan rate of 1 mV/s.

- on the other hand, experiments were performed to monitor the free corrosion potential, E_{CORR}, as a function of time, in media representative for the underground repository conditions, because the OCP-values derived from the CPP curves do not represent the actual value encountered in the underground environment. The E_{CORR} namely depends on the environmental conditions (*e.g.* oxygen content – since the test solutions are purged with pure nitrogen, to remove the oxygen, the values of E_{CORR} may be too low in the case of aerobic measurements), the surface conditions (*e.g.* mass transport), *etc.* Also, an equilibrium is not obtained within the limited time span of a CPP measurement. E_{CORR} has been known to vary with time. Dunn et al. [16] found an increase of ~430 mV in a 1000 mg/L Cl^- solution for alloy 825 over the course of 600 days. The displacement of E_{CORR} in the noble direction with time is thought to be related to passive film thickening and changing film composition [17].

A combination of these two techniques is essential in establishing the corrosion behaviour of the candidate container (overpack) materials. This is realized by comparing the 'actual' value of E_{CORR} relative to E_{NP} and E_{PP}, which are determined from the CPP-curves:

- $E_{CORR} \geq E_{NP}$: immediate pitting problems;
- $E_{CORR} << E_{NP}$: no pitting will occur;
- $E_{CORR} < E_{NP}$: if E_{CORR} is close to E_{NP}, pitting can occur if the separation between E_{CORR} and E_{NP} is reduced, *e.g.* by changing the oxidizing power of the solution, at MnS inclusions (*i.e.* a local site with a higher potential), *etc.*;
- $E_{CORR} << E_{NP}$ and $E_{CORR} > E_{PP}$: the overpack material could suffer long-term corrosion problems because localized attack, once initiated, will not be able to repassivate;
- $E_{CORR} << E_{PP}$: pits can neither grow nor nucleate;

The experimental setup to perform CPP-measurements at 140°C consists of a potentiostat/galvanostat, a computer, and an autoclave. A three-electrode setup is used, *viz.* a working electrode (*i.e.* a sample of the investigated material), a counter electrode (the vessel wall of the autoclave), and a reference electrode (Ag/AgCl). As reference electrode, an internal Ag/AgCl electrode, completely constructed from Teflon®, was developed in cooperation with the Reactor Materials Department of SCK•CEN. The electrode consists of a silver wire onto one end of which a AgCl layer is deposited electrolytically. This wire is placed inside a heat-shrunk Teflon® tube which is filled with 0.1M KCl. A ceramic plug ($MgO\text{-}ZrO_2$) maintains contact between the sensing element of the reference electrode and the test solution. The Teflon® heat shrinkable tubing provides the pressure balance between the internal electrolyte solution and the test solution in the autoclave. A schematic representation of the internal Ag/AgCl reference electrode is shown in Figure 21

2.3.2 Results

Determination of E_{NP} and E_{PP} potentials by cyclic potentiodynamic polarization (CPP) measurements

The results from the CPP-measurements on the candidate container materials (carbon steel TStE 355, stainless steels AISI 316L, AISI 316Ti, AISI 316L hMo, and UHB 904L, nickel alloys Hastelloy C-4 and C-22, and Ti-alloy Ti/0.2PD) in SOCW-solutions at 140°C under aerobic conditions are presented in Table 17. The Table contains data for the critical potential for pit nucleation, E_{NP} (values in bold), and the protection potential, E_{PP2} (values between brackets). Some of the results are missing in the table because these experiments were performed during the 2nd half of September and could, therefore, not be interpreted within the framework of this reporting period.

Ti/0.2Pd is the only tested candidate container material that is resistant to pitting corrosion in all SOCW-solutions (100 - 50,000 mg/L Cl^-). Carbon steel is attacked by uniform corosion in all SOCW-solutions (100 - 50,000 mg/L Cl^-).

The recorded CPP-curves for Hastelloy C-4 and Hastelloy C-22 show the presence of a positive hysteresis in several SOCW-solutions. This shape is generally associated with the onset of pitting corrosion on the test sample. However, surface analyses (Optical Microscopy and Scanning Electron Microscopy) indicate that Hastelloy C-4 and C-22 are not attacked by pitting corrosion:

- ***HASTELLOY C-4.*** In SOCW-solutions up to 20,000 mg/L Cl^-, the surface of the samples only revealed a tarnished surface, *i.e.* a yellow-orange discolouration of the surface, without evidences of pitting attack. In SOCW-solutions containing 20,000 mg/L Cl^- and higher, evidence of attack was only observed at the interface between the sample and the mounting resin, as can be seen in Figure 22, while the rest of the sample remained unaffected. Therefore, it was concluded that in these high chloride containing solutions, the hysteresis was due to crevice corrosion. EDS-analysis of the attacked zone (zone 1, square) only revealed the presence of the major alloying elements of HASTELLOY C-4 (Ni, Cr, Mo, Fe). EDS-analysis of the layer (zone 2, circle) adjacent to the attacked zone revealed the presence of K, Na, and Cl, indicating that this layer mainly consists of salt deposits of the test solution (NaCl, KCl), together with some of the alloying elements (Ni, Cr, Mo).

- ***HASTELLOY C-22.*** In SOCW-solutions with a chloride concentration lower than 50,000 mg/L, no hysteresis was found on the CPP-curves and no alteration of the surface (neither tarnishing nor corrosion attack) was observed. Figure 23 shows a SEM-micrograph of an uncleaned HASTELLOY C-22 sample after CPP-testing in SOCW containing 216 mg/L SO_4^{2-} and 50,000 mg/L Cl^-. A thick salt layer was observed near the interface sample/mounting resin. EDS-analysis of this layer (zone 3, rectangle) revealed the presence of remnants of the test solution (K, Na, and Cl) together with some of the alloying elements (Ni, Cr, Mo). However, at the top right of zone 3 (indicated with the arrow) slight signs of crevice corrosion are observed (see the typical circular shaped attack).

Influence of alloying elements, chloride and sulphate concentration on the pitting susceptibility of AISI 316L, AISI 316L hMo, AISI 316Ti, and UHB 904L

Figure 24 and Figure 25 present the data for E_{NP} as a function of Cl^- for AISI 316L, AISI 316L hMo, AISI 316Ti, and UHB 904L type stainless steels in SOCW containing 216 mg/L SO_4^{2-} and 5,400 mg/L SO_4^{2-}, respectively. In SOCW containing 216 mg/L SO_4^{2-} and 100 mg/L Cl^-, E_{NP} is more than 200 mV more positive than the actual E_{CORR} (+320 mV_{SHE}) for all tested stainless steels. These materials are therefore unlikely to suffer pitting immediately after closure of the underground repository under normal disposal conditions in the Boom clay formation (140°C, presence of oxygen, 90 mg/L Cl^-). When Cl^- is increased to 1,000 mg/L than only UHB 904L will remain resistant to pitting in SOCW containing 216 mg/L SO_4^{2-} (E_{NP} is still about 200 mV more noble than the actual E_{CORR}). In SOCW containing 5,400 mg/L SO_4^{2-} and 100 mg/L Cl^-, none of the stainless steels showed signs of pitting attack. When $[Cl^-]$ is increased to 1,000 mg/L than still all the stainless steels are resistant to pitting. However, when $[Cl^-]$ is increased even further to 10,000 mg/L than only UHB 904L is resistant to pitting.

In all test solutions (216 mg/L and 5,400 mg/L SO_4^{2-}), the protection potential was more negative than the actual E_{CORR} for all stainless steels. This implies that once the protective layer is damaged locally, the environmental conditions are such that it will not be able to repassivate.

From Figures 24 and 25, the following conclusions can be drawn:

- UHB 904L has a slightly higher resistance to pitting than the other tested stainless steels. E_{NP} is always more than 200-300 mV more positive for UHB 904L in comparison to the other stainless steels.

- the three grades of AISI 316 type stainless steel (AISI 316L, AISI 316L hMo, and AISI 316Ti) have comparable pitting characteristics. The E_{NP}-values usually differ less than 100 mV.

- the pitting resistance of all tested stainles steels decreases with increasing chloride concentration. E_{NP} is drastically shifted towards more active potentials with increasing Cl^-.

- sulphate has an inhibiting effect on pitting: in SOCW containg 5,400 mg/L SO_4^{2-}, more chloride is needed to initiate pitting. This inhibiting effect, however, diminishes as Cl^- increases. The E_{NP}-values are comparable in SOCW containing 216 and 5,400 mg/L SO_4^{2-} when $[Cl^-]$ is 10,000 mg/L or higher for AISI 316L, AISI 316L hMo, and AISI 316Ti. For UHB 904L, the inhibiting effect of SO_4^{2-} only disappears at very high $[Cl^-]$ (50,000 mg/L).

Estimation of the maximum chloride level above which pitting is expected to occur

It has been found [18,19] that a linear relationship exists between the critical pit nucleation potential, E_{NP}, and the chloride concentration, $[Cl^-]$, of the type

$$E_{NP} = A - B \cdot \log[Cl^-] \quad (1)$$

where B is a constant depending on the alloy composition, supporting electrolyte composition, measurement technique, *etc.*

From equation (1), it is possible to estimate the maximum chloride level above which pitting is expected to occur immediately in environments relevant for various underground repository conditions (conditions evolving in the course of the disposal period). The maximum chloride level is determined as the intersection between the regression line and the actual value of E_{CORR}. In SOCW under aerobic conditions, E_{CORR} is +320 mV_{SHE}.

The regression lines and the fitting results for AISI 316L, AISI 316L hMo, AISI 316Ti, and UHB 904L type stainless steels in SOCW containing 216 and 5,400 mg/L SO_4^{2-} under aerobic conditions (140°C) are presented in Figures 26 and 27, respectively. The estimated chloride levels above which pitting is expected to occur immediately in SOCW under aerobic conditions at 140°C are shown in Table 18. For comparison, the results for 90°C (originating from the previous EC-Project) are added The following conclusions can be drawn from Table 18:

- all four tested stainless steels seem to be adequately resistant to pitting corrosion in an argillaceous environment under aerobic conditions. Under the most severe conditions, i.e. high temperature (140°C) and low degree of oxidation (216 mg/L SO_4^{2-}), the maximum level of chloride above which pitting is not expected to occur for AISI 316L is approximately 560 mg/L, which is more than 6 times higher than the expected chloride content of the near-field environment for the Belgian disposal concept (~90 mg/L Cl^-). The other three stainless steels can even resist environments containing higher amounts of Cl^-. Cl^-_{max} for AISI 316L, AISI 316Ti, and AISI 316L hMo was estimated to be 980, 1220, and 10800 mg/L, respectively).

- as the near-field environment becomes more oxidized, i.e. the further in the disposal period, the tested stainless steels become more resistant to pitting. Cl^-_{max} increases by a factor of about 6-7 (140°C) when [SO_4^{2-}] increases from 216 to 5,400 mg/L. This effect is most pronounced at 140°C and is almost negligible at 90°C.

Influence of temperature

The influence of temperature on the pitting susceptibility of AISI 316L, AISI 316Ti, AISI 316L hMo, and UHB 904L type stainless steel in SOCW containing 216 and 5,400 mg/L SO_4^{2-} is presented in Figures 28 and 29. The Figures show that the increase of temperature from 90 to 140°C lowers E_{NP} by several hundreds of millivolts. This decrease of E_{NP}, as a consequence of an increasing temperature, becomes smaller with increasing Cl^-. Also the influence of temperature on the values of E_{NP} is less pronounced for UHB 904L. Figures 28 and 29 also show that AISI 316L, AISI 316Ti, and AISI 316L hMo type stainless steels present rather similar pitting resistance characteristics.

From Table 18 it can also clearly be seen that when the temperature is increased from 90 to 140°C, the maximum chloride level above which pitting is not expected to

occur decreases drastically. At 216 mg/L SO_4^{2}, Cl^-_{max} decreases approximately 15, 10, and 8 times for AISI 316L, AISI 316Ti, and AISI 316L hMo, respectively. In highly oxidizing clay environments (5,400 mg/L SO_4^{2-}), the temperature has a much lower influence on Cl^-_{max}. UHB 904L is less susceptible to temperature than the other stainless steels investigated.

3. CONCLUSIONS

From the results obtained in these studies, the following conclusions can be drawn:

- In the $MgCl_2$-rich Q-brine (T=150°C) and in the absence of gamma radiation, no contact corrosion occurs on the material pair Ti99.8-Pd and TStE355 carbon steel. The general corrosion rates of the coupled Ti99.8-Pd and carbon steel specimens correspond very well to the values of the uncoupled specimens. Furthermore, the coupled specimens are resistant to pitting corrosion as do also the uncoupled speciments. In the presence of a gamma radiation field of 10 Gy/h in the brine, a strong contact corrosion occurs. This results in the case of the coupled carbon steel to severe local corrosion attacks and to a significant increase of its corrosion rate, compared to the value of the uncoupled steel specimens. The high increase in the corrosion rate of the coupled steel specimens under irradiation is attributed to the fact that the oxidants, mainly O_2, formed by the radiolysis of water are reduced at the Ti99.8-Pd cathode, which results to an increase of the oxidation rate of Fe.

- Cu and the Cu-Ni alloys 90-10 and 70-30 exhibit in NaCl-rich brine a uniform corrosion with low corrosion rates (3-12 µm/a). The imposition of a gamma radiation field of 10 Gy/h decreases the corrosion rate in this brine. In the $MgCl_2$-rich Q-brine, the materials are subject to non-uniform corrosion and the corrosion rates (24-46 µm/a) are clearly higher than in the NaCl-rich. In addition, intergranular corrosion was observed on Cu and the alloy Cu-Ni 90-10.

- Electrochemical studies performed at rest potentials in salt brines at 25°C and 80°C show in agreement with the long-term immersion experiments that at both temperatures the corrosion rates of carbon steel, Cu, Ni, and Cu-Ni alloys (90-10 and 70-30) in Q-brine are higher than in NaCl-rich brine, except of Ni at 80°C. The increase of temperature from 25°C to 80°C increases the corrosion rate of the materials. Furthermore, it can be stated that the corrosion rate of Ni in both brines is smaller than that of Cu, and that the higher the Ni content of the Cu-Ni alloys the higher their resistance to corrosion. Contact corrosion studies on material pairs such as carbon steel in contact with Cu, Ni,and Cu-Ni alloys or Cu in contact with Ni show that the contact corrosion potential is dominated by the less noble partner, i.e., carbon steel or Cu in contact with Ni.

- In granitic water with a low chloride concentration (98 mg/l) at 90°C, the carbon steel TStE355 exhibits a sufficient resistance to pitting corrosion, and its general corrosion rate is relatively low (21 µm/a). However, in granitic-bentonite water with high chloride concentration (6260 mg/l), the steel suffers from severe pitting corrosion. The results of Slow Strain Rate Tests (SSRT), electrochemical studies, and crevice corrosion experiments at 90°C in granitic-bentonite water containing up to 50000 ppm chloride show that the materials Hastelloy C-22 and Cu both in

unwelded and welded condition are resistant to stress corrosion cracking (SCC), pitting and crevice corrosion. The alloy Cu-Ni 70-30 is also resistant to pitting and crevice corrosion at 90°C, but it shows in the granitic environment containing a very high chloride concentration of 50000 ppm a slight susceptibility to SCC at the very slow strain rates of 10^{-6} s^{-1} and $2x10^{-7}s^{-1}$.

- In clay water (aerobic conditions, 100-50000 mg/l Cl^-) at 140°C, the corrosion allowance material TStE355 carbon steel is subject to uniform corrosion. Among the passively corroded materials (stainless steels, Ni-base alloys and Ti99.8-Pd), only the alloy Ti99.8-Pd is resistant to pitting corrosion under all test conditions applied. The Ni-base alloys Hastelloy C-4 and Hastelloy C-22 exhibit also a high resistance to pitting corrosion in clay water containing up to 20000 mg/l Cl^-. At higher Cl^- concentrations slight crevice corrosion was observed. The stainless steels (AISI 316L, AISI 316L hMo, AISI 316Ti, and UHB 904L), have a lower resistance to pitting corrosion than the Ni-base alloys. However, pitting corrosion occurs on the steels at Cl^- contents, which are significantly higher than the Cl^- content expected in the near-field environment of the Belgian disposal concept.

4. REFERENCES

[1] G.P. Marsh, G. Pinard-Legry, E. Smailos et al., “HLW Container Corrosion and Design,” Proc. of the Second European Community Conf. and Radioactive Waste Management and Disposal, Luxembourg, April 22-26, 1985, p.314, R.A. Simon (Ed.), Cambridge University Press, EUR 13389 (1986).

[2] E. Smailos, W. Schwarzkopf, R. Köster and K.H. Grünthaler, ”Advanced Corrosion Studies on Selected Packaging Materials for Disposal of HLW Canisters in Rock Salt,” Proc. of the Symposium on Waste Management 1988, Tucson, Arizona, USA, February 28-March 3, 1988, Vol.2, pp. 985-994, Arizona Board of Regents (1988).

[3] E. Smailos, I. Azkarate, J.A. Gago, P. Van Iseghem, B. Kursten, T. McMenamin, ”Corrosion Studies on Metallic HLW Container Materials, ”Proc. of the 4th European Conf. on Management and Disposal of Radioactive Waste, Luxembourg, 25-29 March 1996, pp. 209-223, T.McMenamin (Ed.), EUR 17543 (1997).

[4] E. Smailos, W. Schwarzkopf and R. Storch, ”Corrosion Studies on Packaging Materials for High-Level Waste Disposal in a Rock-Salt Repository,” Proc. of the 12th Scandinavian Corrosion Congress and Eurocorr ’92, Espoo, Finland, June 1992, pp. 327-338 (1992).

[5] E. Smailos, A. Martínez-Esparza, B. Kursten, G. Marx, I. Azkarate, ”Corrosion Evaluation of Metallic Materials for Long-Lived HLW/Spent Fuel Disposal Containers,” EUR-Report 19112 (1999).

[6] E. Smailos, “Investigation of the contact corrosion between the candidate hlw/spent fuel disposal container materials Ti-Pd and carbon steel in NaCl-rich brine,” Proc. of the International Conference UK CORROSION 2002, 22-24 October 2002, Cardiff, Wales.

[7] H. Kaesche,” Die Korrosion der Metalle”, Springer Verlag, Berlin-Heidelberg-New York (1979).

[8] H. Remy, Lehrbuch der Anorganischen Chemie, Leipzig, 1959, p.373.

[9] "Preparation of a synthetic granitic-bentonite water". Specific procedure no. PR-X8-01, CIEMAT, 1996.

[10] Corrosion of metals and alloys – Stress corrosion testing. Part 7: Slow strain rate testing”. ISO 7539-7, International Standard ISO 1989-12-01.

[11] Standard Practice for Slow Strain Rate Testing to Evaluate the Susceptibility of metallic Materials to Environmentally Assisted Cracking”, Standard G129- , Annual Book of ASTM Standards, Vol.03.01; West Conshohocken, PA, ASTM.

[12] “Standard Reference Test Method for Making Potentiostatic and Potentiodynamic Anodic Polarization Measurements”. Standard G5-, Annual Book of ASTM Standards, Vol.03.02; West Conshohocken, PA, ASTM.

[13] “Corrosion of metals and alloys – Electrochemical test methods – Guidelines for conducting potentiostatic and potentiodynamic polarization measurements”. COMMITTEE DRAFT, ISO/CD 17475, International Standard ISO 2001.

[14] “Standard Practice for Calculation of Corrosion Rates and Related Information from Electrochemical Measurements”. Standard G102- , Annual Book of ASTM Standards, Vol.03.02; West Conshohocken, PA, ASTM.

[15] “Crevice Corrosion Testing of Iron-Base and Nickel- Base Stainless Alloys in Seawater and other Chloride-Containing Aqueous Environments”. Standard G78- , Annual Book of ASTM Standards, Vol.3.01; West Conshohocken, PA, ASTM.

[16] D.S. Dunn, G.A. Cragnolino, and N. Sridhar,”An Electrochemical Approach to Predict Long-Term Localized Corrosion of Corrosion-Resistant High-Level Waste Container Materials, ” *Corrosion* **56** (1), pp. 90-104 (2000).

[17] J.-H. Wang, C.C. Su, and Z. Szklarska-Smialowska,”Effects of Cl^- Concentration and Temperature on Pitting of AISI 304 Stainless Steel,” *Corrosion* **44** (10), pp. 732-737 (1988).

[18] Z. Szklarska-Smialowska, "Pitting corrosion of metals," NACE International,1986 Houston Texas, USA.

[19] A.J. Sedriks, "Corrosion of stainless steels," 2nd edition, Wiley-Interscience, New York, USA (1996).

5. MANAGEMENT AND CO-ORDINATION ASPECTS

Co-ordination was carried out in accordance with the obligations specified in Article 2 of Annex II to the contract (see also session 4.3 of Annex I to the contract).

Project Co-ordination meetings (PCM) were held on:

- 22-23 May 2002 in Madrid. The minutes of the meeting were submitted to the EC in June 2002.
- 11-12 October 2002 in Berlin. The minutes of the meeting were submitted the EC in November 2002.

In accordance with the contract, the following reports were submitted to the EC:

The First Annual Report, the advanced version of the Technology Implementation Plan (TIP), and the Mid-Term Report.

6. DEPARTURES FROM THE WORK PLAN

The updated time schedule of the work plan is shown in Annex.

The activities related to the work packages WP1 (Corrosion studies in salt environments; FZK.INE and GNF.IUT), WP2 (Corrosion studies in granitic environments; ENRESA/INASMET and FZK.INE) and WP3 (Corrosion studies in clay environments, SCK.CEN) have been performed according to the time schedule given in the Technical Annex to the contract.

7. PLANNED ACTIVITIES FOR THE NEXT REPORTING PERIOD

Corrosion studies in salt environments (WP1)

- Investigation of the contact corrosion between the Cu-base materials and carbon steel in salt brines.

- Characterization of the corrosion layers formed on the surface of corroded specimens of carbon steel, Cu, Ni and Cu-Ni alloys

Corrosion studies in granitic-bentonite environments (WP2)

- Long-term corrosion studies on Cu-base materials.

- Slow strain rate tests on welded Cu-specimens.

- Conclusion of the crevice corrosion studies on welded Hasteloy C-22, Cu and Cu-Ni 70-30.

Corrosion studies in clay environments (WP3)

- Completion of the aerobic experiments on the preselected container materials at 140°C in synthetic bentonite water (SBW).

8. LIST OF DISTRIBUTED PAPERS

Title	Date	Addressee
1st Annual Report	November 2001	EC,Partners
Cost Statements 1st year	December 2001	EC
TIP (at Mid-Term)	March 2002	EC, Partners
Mid-Term Report	March 2002	EC, Partners
Minutes 3rd PCM	June 2002	Partners, EC
Minutes 4th PCM	November 2002	Partners, EC

TIP = Technology Implementation Plan
PCM = Project Coordination Meeting

Table 1: Corrosion rates of coupled and uncoupled Ti99.8-Pd and TStE355 steel in $MgCl_2$-rich brine (Q-brine) at 150°C

Material	Corrosion conditions	Corrosion rate (µm/a)	
		coupled specimens	uncoupled specimens
Ti99.8-Pd	Q-brine	0.08 ± 0.02	0.02 ± 0.01
	Q-brine/10 Gy/h	0.25 ± 0.02	0.20 ± 0.02
TStE355 steel	Q-brine	36.6 ± 14.5	47.1 ± 2.5
	Q-brine/10 Gy/h	369.5 ± 46.7	72.6 ± 11.0

Table 2: Linear corrosion rates of Cu-base materials in NaCl-rich brine at 150°C

Material	Linear corrosion rate (µm/a)	
	without γ-radiation	with γ (10 Gy/h)
Cu	3.0 ± 0.5	0.4 ± 0.3
Cu-Ni 90-10	11.8 ± 0.6	0.8 ± 0.6
Cu-Ni 70-30	4.2 ± 0.4	1.3 ± 0.7

Table 3: Linear corrosion rates of Cu-base materials in the $MgCl_2$-rich Q-brine at 150°C

Material	Corrosion rate (µm/a)
Cu	24.4 ± 2.6
Cu-Ni 90-10	37.0 ± 4.7
Cu-Ni 70-30	46.0 ± 2.0

Table 4: Corrosion rates of the materials investigated under aerobic conditions in the test brines at rest potential at 25°C

Material	Brine	Rest potential mV (SHE)	Weight loss (mg)	Time (h)	Corrosion rate (µm/a)
Ni	Q-brine	-50 +/- 5	0.1	230	8.6
Ni	NaCl-rich	-106 +/- 8	0.05	70	14
Cu	Q-brine	-124 +/- 5	0.24	193	24
Cu	Q-brine	-120 +/- 5	0.09	78	23
Cu	NaCl-rich	-106 +/- 5	0.17	193	17
Cu	NaCl-rich	-100 +/- 5	0.18	193	18
TStE355 steel	Q-brine	-445 +/- 5	-	155	-
TStE355 steel	Q-brine	-435 +/- 5	0.21	220	22
TStE355 steel	NaCl-rich	-410 +/- 5	-	166	-
TStE355 steel	NaCl-rich	-440 +/- 8	0.13	220	14
Cu-Ni 70-30	Q-brine	-94 +/- 5	0.14	210	13
Cu-Ni 70-30	Q-brine	-130 +/- 5	0.20	225	17
Cu-Ni 70-30	NaCl-rich	-27 +/- 4	0.05	180	5.5
Cu-Ni 90-10	Q-brine	-123 +/- 4	0.15	96	31
Cu-Ni 90-10	NaCl-rich	-126 +/- 4	0.05	70	14

Table 5: Corrosion rates of the materials investigated under aerobic conditions in the test brines at rest potential at 80°C

Material	Brine	Rest potential mV (SHE)	Weight loss (mg)	Time (h)	Corrosion rate (µm/a)
Ni	Q-brine	-115 +/- 10	0.58	77	148
Ni	NaCl-rich	-130 +/- 8	0.84	77	215
Cu	Q-brine	-180 +/- 8	0.45	77	115
Cu	NaCl-rich	-160 +/- 10	0.41	77	105
TStE355 steel	Q-brine	-375 +/- 5	0.73	101.5	166
TStE355 steel	NaCl-rich	-440 +/- 10	0.34	100	78
Cu-Ni 70-30	Q-brine	-156 +/- 5	0.37	80.25	91
Cu-Ni 70-30	NaCl-rich	-100 +/- 10	0.31	80.25	76
Cu-Ni 90-10	Q-brine	-160 +/- 8	0.26	80.25	64

Table 6: Contact potentials and corrosion rates of carbon steel, Cu, Ni and Cu-Ni-alloys in Brines at 25°C at 80°C

Materials/ Brine [1)]	Me [2)] (80°C) Corrosion rate (µm/a)	Steel (80°C) Corrosion rate (µm/a)	Me (25°C) Corrosion rate (µm/a)	Steel (25°C) Corrosion rate (µm/a)	Contact potential. (80°C) mV (SHE)	Contact potential (25°C) mV (SHE)
Ni/Steel-Q	11 (Ni)	510	*	42	-380	-428
Ni/Steel-Brine 3	4 (Ni)	315	*	45	-438	-448
Cu/Steel-Q	13 (Cu)	342	5	33	-385	-427
Cu/Steel-Brine 3	19 (Cu)	253	*	42	-420	-449
Cu-Ni 70-30/Steel Q	12 (Cu-Ni 70-30)	598	37	61	-382	-428
Cu-Ni 70-30/Steel Brine 3	27 (Cu-Ni 70-30)	276		89	-438	-446
Cu-Ni 90-10/Steel Q	31 (Cu-Ni 90-10)	429	36	73	-395	-419
Cu-Ni 90-10/Steel Brine 3	35 (Cu-Ni 90-10)	333	33	58	-425	-442
	Corrosion rate Cu (80°C) (µm/a)	Corrosion rate Ni (80°C) (µm/a)	Corrosion rate Cu (25°C) (µm/a)	Corrosion rate Ni (25°C) (µm/a)	Contact potential Cu/Ni (80°C) MV (SHE)	Contact potential Cu/Ni (25°C) mV (SHE)
Cu/Ni-Q	154	76	43	*	-165	-111
Cu/Ni-Brine 3	189	24	49	*	-110	-107

*) no detected

[1)] Q-brine = $MgCl_2$-rich brine; Brine 3 = NaCl-rich brine

[2)] Me = Ni, Cu, Cu-Ni 90-10, Cu-Ni 70-30, respectively

Table 7: Corrosion rates of the investigated materials obtained from surface treated and untreated electrodes under aerobic conditions at rest potentials at 80°C

Material	Brine	Restpotential mV (SHE)	Weight loss (mg)	Time (h)	Rate (µm/a)
Ni	Q-brine (A)[1)]	-115 +/-10	0.58	77	148
Ni	Q-brine (B)[2)]	-120 +/- 10	0.12	103	23
Ni	NaCl-brine (A)	-130 +/- 8	0.84	77	215
Ni	NaCl-brine (B)	-145 +/- 8	0.01	103	2
Cu	Q-brine (A)	-180 +/- 8	0.45	77	115
Cu	Q-brine (B)	-155 +/- 10	0.5	103	95
Cu	NaCl-brine (A)	-160 +/-10	0.41	77	105
Cu	NaCl-brine (B)	-170 +/- 8	0.12	103	23
TStE 355 steel	Q-brine (A)	-375 +/-7	0.73	101.5	166
TStE 355 steel	Q-brine (B)	-405 +/- 10	0.02	102	5
TStE 355 steel	NaCl-brine (A)	-440 +/- 10	0.34	100	78
TStE 355 steel	NaCl-brine (B)	-460 +/- 10	0.02	102	5
Cu-Ni 70-30	Q-brine (A)	-156 +/- 5	0.37	80.25	91
Cu-Ni 70-30	Q-brine (B)	-110 +/- 10	*	102	*
Cu-Ni 70-30	NaCl-brine(A)	-100 +/-10	0.31	80.25	76
Cu-Ni 70-30	NaCl-brine (A)	-135 +/- 8	0.13	101.5	25
Cu-Ni 70-30	NaCl-brine (B)	-60 +/- 8	*	102	*
Cu-Ni 90-10	Q-brine (A)	-160 +/-8	0.26	80.25	64
Cu-Ni 90-10	Q-brine (B)	-175 +/- 8	0.28	100.5	55
Cu-Ni 90-10	Q-brine (B)	-190 +/- 8	0.24	100.5	47
Cu-Ni 90-10	NaCl-brine (B)	-195 +/- 8	0.14	100.5	27
Cu-Ni 90-10	NaCl-brine (B)	-180 +/- 5	0.11	100.5	22

*) no detected

1) A = correct data obtained from surface treated electrodes ; [2)] B = wrong data obtained from surface untreated electrodes

Table 8: Composition of granitic water 1 (low Cl^- concentration) used in the long-term corrosion experiments (CEA reference water)

Ion	Concentration (mg/l)
Na^+	97.20
Ca^{2+}	2.30
K^+	4.60
Al^{3+}	1.40
Li^+	0.10
B^{3+}	0.08
Cl^-	98.10
HCO_3^-	25.60
$H_3SiO_4^-$	39.40
F^-	4.90

pH(22°C)=9.1

Table 9: Composition of granitic water 2 (high Cl^- concentration) used in the long-term corrosion experiments (CIEMAT reference water)

Ion	Concentration (mg/l)
Na^+	3883.0
Ca^{2+}	151.9
Mg^{2+}	577.7
K^+	20.8
Si	3.4
Cl^-	6258.5
SO_4^{2-}	1304.7
HCO_3^-	34.0
NO_3^-	111.4
Br^-	15.0

pH(22°C)=7.3

Table 10: Corrosion results obtained for the TStE355 carbon steel in granitic waters at 90°C (V/S = 2ml/cm^2)

Granitic water 1 (98 mg/l Cl^-)			Granitic water 2 (6260 mg/l Cl^-)		
Exposure time (d)	Linear corrosion rate (µm/a)	Max. pit depth (µm)	Exposure time (d)	Linear corrosion rate (µm/a)	Max. pit depth (µm)
84	21.1±2.1	25	83	22.6±3.6	250
147		50	161		900
223		60	300		1200
308		60	460		1300

Table 11: Corrosion of TStE355 steel in granitic water 2 (high Cl^- concentration of 6260 mg/l) after 460 days at 90°C - Results of Fe-analyses of corrosion solution and solid corrosion products

Fe-analyses of	IC			ICP-AES
	Fe^{2+} (mg/l)	Fe^{3+} (mg/l)	Fe_{tot} (mg/l)	Fe_{tot} (mg/l)
unfiltered brine	< 0.1	0.4	0.4	0.3
filtered brine (0.45 µm)	<0.1	1.5	1.5	0.3
filtered brine (1.8 nm)	<0.1	0.6	0.6	0.8
corrosion product on specimen	3939	5662	9601	10250
corrosion product on the bottom of vessel	608	10016	10624	10635

Table12. Chemical composition of the materials investigated in the localized corrosion experiments

Composition (weight %)	HC-22 (UNS N06022)		Cu-OF (UNS C10200)		Cu30Ni (UNS C71500)	
	Plate	Bar	Plate	Bar	Plate	Bar
Ni	*Base*	*Base*	<0.01	<0.01	30.2	30.0
Cr	21.8	21.6				
Mo	13.3	13.0				
W	3.0	3.0				
Fe	2.8	2.9	<0.01	<0.01	0.65	0.73
Cu	0.03	0.08	*Base*	*Base*	*Base*	*Base*
Co	0.38	0.95				
Al	0.22	0.19			<0.01	<0.01
V	0.16	0.14				
C	0.014	0.003			0.005	0.020
Mn	0.22	0.26	<0.01	<0.01	0.69	0.68
P	0.01	<0.01	<0.01	<0.01	<0.01	0.01
O			0.019	0.027	0.006	0.005

Table 13. Composition of simulated granitic-bentonite water used in the localized corrosion experiments

Parameter	Composition (mg/l)
Cl^-	6500 - 50000
NO_3^-	110±10
SO_4^{2-}	1500±30
HCO_3^-	27±5
SiO_2	8.3±0.5
Br^-	15±1
Ca^{2+}	135±10
K^+	20±1
Mg^{2+}	600±30
Na^+	3750±100
pH (25ºC)	7.3

Table 14: Summary of SSRT data obtained for the Cu30Ni alloy tested in argon and granite with different chloride contents at strain rates of 10^{-6} and $2x10^{-7}s^{-1}$

Cu30Ni	Argon 10^{-6} s^{-1}	G/6500 Cl^- 10^{-6} s^{-1}	G/ 50000 Cl^- $10^{-6}s^{-1}$	Argon $2x10^{-7}s^{-1}$	G/6500 Cl^- $2x10^{-7}s^{-1}$	G/50000 Cl^- $2x10^{-7}s^{-1}$
Elongation (%)	52	49	48	53	54	53
Reduction of area (%)	69	69	70	74	72	69
Yield strength (MPa)	119	110	118	157	145	134
Maximum Load (MPa)	307	306	303	344	321	319
True Stress at Fracture (MPa)	726	716	717	895	782	692
Time to rupture (hr)	155	148	143	795	878	789
Maximum crack penetration (μm)	-	65	120	-	80	120
Fracture mode	Ductile	Ductile +Intergr[1]	Ductile .+Intergr[1]	Ductile	Ductile +Intergr[1]	Ductile +Intergr[1]

G= granitic-bentonite water; 1) intergranular areas

Table 15: Corrosion data from electrochemical polarization tests.

Material	Cl^- (ppm)	Ecorr (V)		Corr.rate (μm/a)		Surface appearance	
		25ºC	90ºC	25ºC	90ºC	25ºC	90ºC
Cu-OF	6550	-0.28	-0.51	11	13	General corrosion (GC)	
	15000	-0.34	-0.37	14	70	General corrosion	
	50000	-0.32	-0.42	86	140	General corrosion	
Cu30Ni	6550	-0.26	-0.33	21	70	Bright / light scale	
	15000	-0.20	-0.38		70	GC/dealloying	light scale/ GC
	50000	-0.35	-0.40	65	390	GC/dealloying	light scale/ GC
Cu30Ni / EBW	50000		-0.40		87	-	light scale/ GC
Cu30Ni / GTAW	50000		-0.39		44	-	light scale/ GC
HC-22	6550	-0.41	-0.30	<10	15	Bright / passive scale	
	15000	0.37	-0.35	<10	18	Bright / passive scale	
	50000	0.25	-0.33	<10	14	Bright / passive scale	
HC-22 / EBW	50000		-0.17			Bright / passive scale	
HC-22 / GTAW	50000		-0.25			Bright / passive scale	

Table 16: Chemical composition of the candidate container materials investigated in clay environments (wt.%)

	Chemical composition (wt%)										
	Fe	Cr	Ni	Mo	Mn	Si	Ti	C	S	P	Others
Carbon steel											
TStE 355	bal	0.030	0.030	-	1.12	0.344	0.003	0.180	0.002	0.010	Nb 0.017; N_2: 0.005
Stainless steel											
AISI 316L	bal	16.90	11.00	2.08	1.54	0.54	-	0.017	0.001	0.032	
AISI 316Ti	bal	16.80	10.70	2.05	1.08	0.40	0.3	0.044	0.009	0.028	
UHB 904L	bal	19.70	25.00	4.47	1.48	0.19	-	0.019	0.001	0.019	Cu:1.51;N_2:0.080
Nickel alloys											
Hastelloy C4	0.98	15.75	bal.	15.85	0.04	0.02	<0.01	0.003	0.003	0.004	Co:0.01
Hastelloy C22	2.8	21.8	bal.	13.3	0.22	-	-	0.014	0.005	0.01	Co:0.38;W:3.0
Titanium alloy											
Ti/0.2Pd	0.04	-	-	-	-	-	bal	0.01	-	-	Pd:0.16;O_2:0.13; N_2<0.01;H_2:0.001

Table 17: Data (E_{NP}- and E_{PP}-values) from the CPP-measurements.

Solutions	Chemical composition			Stainless steel				Ni-alloy	
	$[Cl^-]$	$[SO_4^{2-}]$	$[S_2O_3^{2-}]$	316L	316L hMo	316Ti	904L	HAST. C-4	HAST. C-22
SOCW1	100	216	0	**491** (-124)	**569** (-110)	**530** (-159)	**1023** (10)	no pitting	no pitting
SOCW2	1,000	216	0	**214** (-156)	**266** (-199)	**265** (-177)	**511** (-181)	no pitting	no pitting
SOCW3	10,000	216	0	**94** (-247)	**172** (-153)	**124** (-309)	**326** (-151)	**363** (-208)	no pitting
SOCW4	20,000	216	0	**52** (-226)	**87** (-284)	**90** (-336)	**256** (-191)	**330** (-222)	no pitting
SOCW5	50,000	216	0	**-15** (-372)	**-2** (-325)	**74** (-350)	**150** (-246)	**342** (-183)	**334** (-101)
SOCW6	100	5,400	0	no pitting	no pitting	no pitting	no pitting	no pitting	no pitting
SOCW7	1,000	5,400	0	**555** (-114)	**680** (-144)	**549** (-145)	**581** (-189)	no pitting	no pitting
SOCW8	10,000	5,400	0	**121** (-187)	**147** (-336)	**218** (-412)	**425** (-279)	no pitting	no pitting
SOCW9	20,000	5,400	0	**62** (-190)	**136** (-333)	**141** (-344)	**347** (-397)	**401** (-188)	no pitting
SOCW10	50,000	5,400	0	**-8** (-276)	**69** (-279)	**133** (-343)	**197** (-204)	**301** (-204)	**348** (-118)
SOCW11	1,000	216	20	**301** (-128)	**301** (-154)	**269** (-153)	**391** (-202)	no pitting	no pitting
SOCW12	1,000	216	50	**239** (-145)	**267** (-213)	**276** (-180)	**522** (-134)	no pitting	no pitting
SOCW13	1,000	216	100	**74** (-190)	**282** (-202)	**285** (-172)	**475** (-165)	no pitting	no pitting
SOCW14	1,000	216	200	**69** (-184)	**153** (-204)	**277** (-207)	**554** (-128)	no pitting	no pitting
SOCW15	1,000	5,400	20	(*)	(*)	(*)	**950** (-36)	no pitting	no piting
SOCW16	1,000	5,400	50	(*)	**626** (-149)	(*)	**789** (-37)	no pitting	no pitting
SOCW17	1,000	5,400	100	(*)	(*)	**683** (-278)	**714** (-66)	no pitting	no pitting
SOCW18	1,000	5,400	200	**589** (-238)	**411** (-150)	(*)	**671** (-101)	no pitting	no pitting

(1) the data in bold represent the critical potential for pit nucleation (E_{NP}) ; the data between brackets represent the protection potential (E_{PP2}).

(*) the results of these experiments were not included yet because these experiments were performed during the 2nd half of September and could therefore not be interpreted within the framework of the reporting period.

Table 18: Estimated chloride levels above which pitting is expected to occur immediately in environments relevant for various disposal conditions in clay (the results for 90°C originate from the previous EC-Project).

Material	**T** (°C)	**Condition**	**$[SO_4^{2-}]$** (mg/L)	**$[Cl^-]_{max}$** (mg/L)
AISI 316L	140	Aerobic	216	0.56×10^3
AISI 316Ti	140	Aerobic	216	0.98×10^3
AISI 316L hMo	140	Aerobic	216	1.22×10^3
UHB 904L	140	Aerobic	216	10.80×10^3
AISI 316L	140	Aerobic	5,400	3.98×10^3
AISI 316Ti	140	Aerobic	5,400	5.91×10^3
AISI 316L hMo	140	Aerobic	5,400	6.82×10^3
UHB 904L	140	Aerobic	5,400	20.59×10^3
AISI 316L	90	Aerobic	216	8.1×10^3
AISI 316Ti	90	Aerobic	216	9.2×10^3
AISI 316L hMo	90	Aerobic	216	9.6×10^3
UHB 904L	90	Aerobic	216	18.3×10^3
AISI 316L	90	Aerobic	5,400	13.8×10^3
AISI 316Ti	90	Aerobic	5,400	10.7×10^3
AISI 316L hMo	90	Aerobic	5,400	13.9×10^3
UHB 904L	90	Aerobic	5,400	12.8×10^3

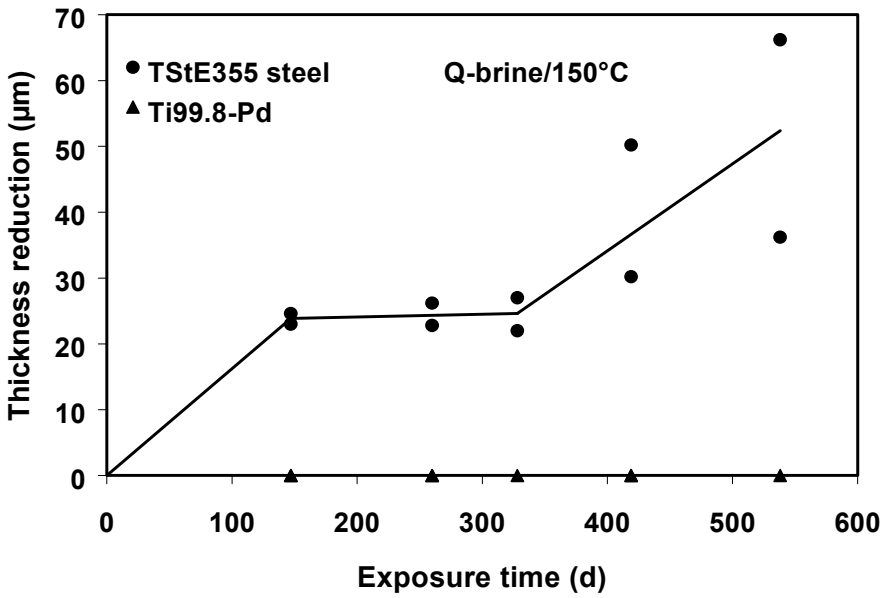

Figure 1: Time-dependence of the thickness reduction of coupled Ti99.8-Pd and TStE355 steel in Q-brine at 150°C

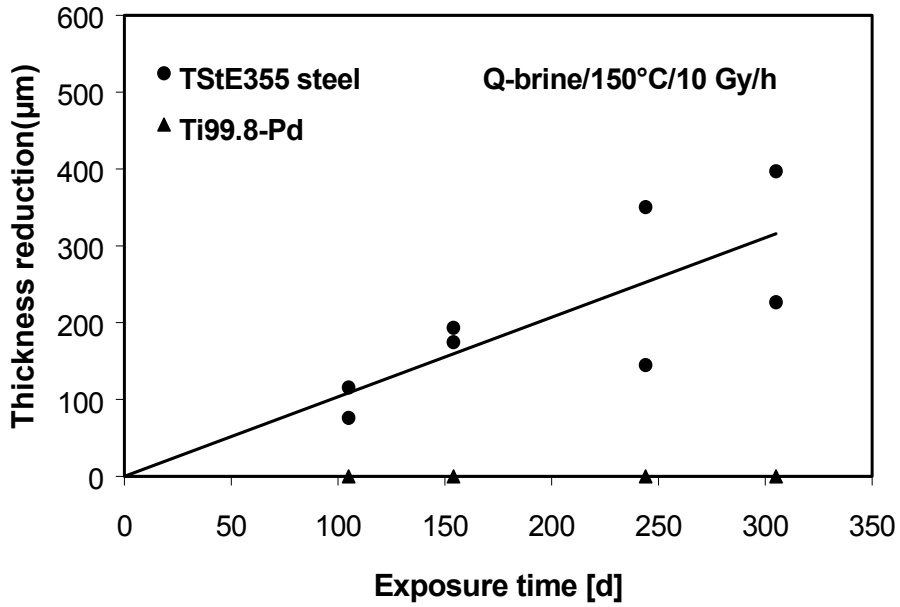

Figure 2: Time-dependence of the thickness reduction of coupled Ti99.8-Pd and TStE355 steel in Q-brine at 150°C and 10Gy/h

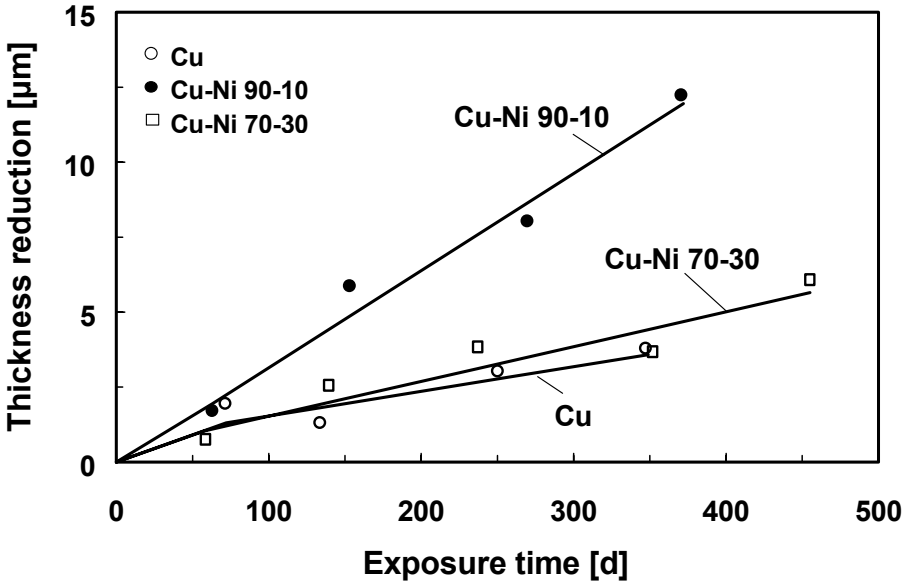

Figure 3: Time-dependence of the thickness reduction of the Cu- base materials in NaCl-rich brine at 150°C

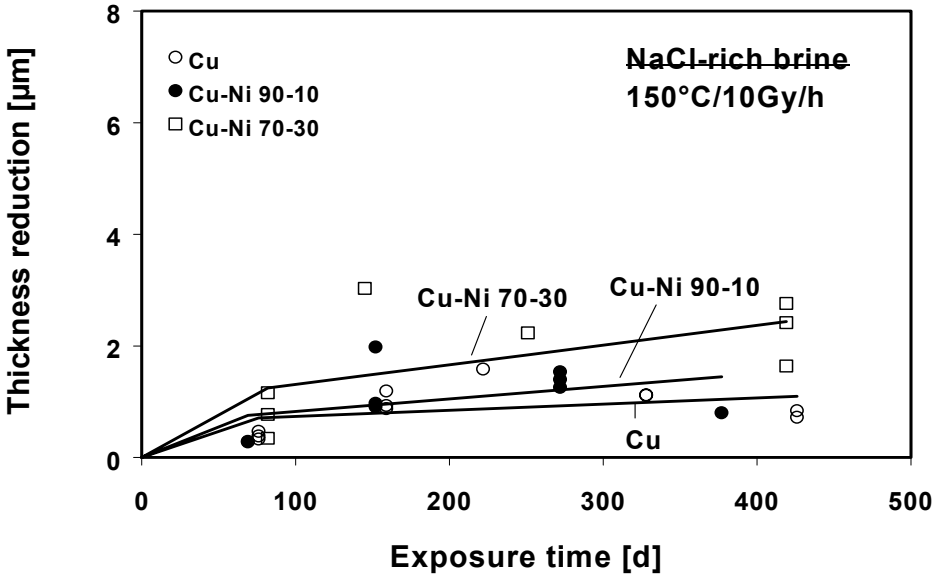

Figure 4: Time-dependence of the thickness reduction of the Cu-base materials in NaCl-rich brine at 150°C and 10 Gy/h

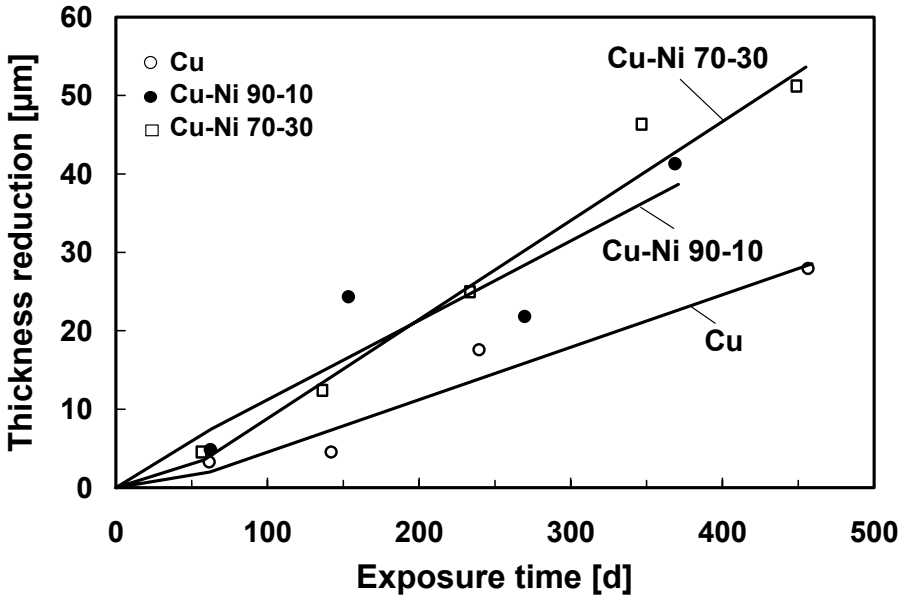

Figure 5: Time-dependence of the thickness reduction of the Cu-base materials at 150°C in the $MgCl_2$-rich brine

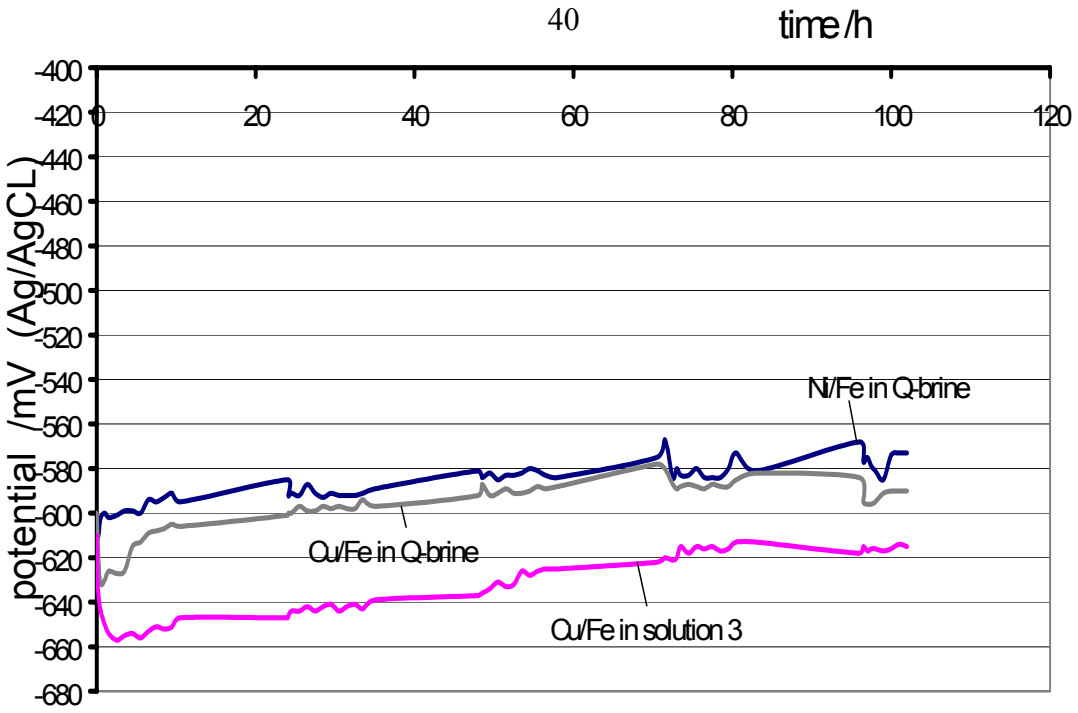

Figure 6: Contact potentials of the material pairs Ni/carbon steel (Ni/Fe) and Cu/carbon steel (Cu/Fe) in brines at 80°C

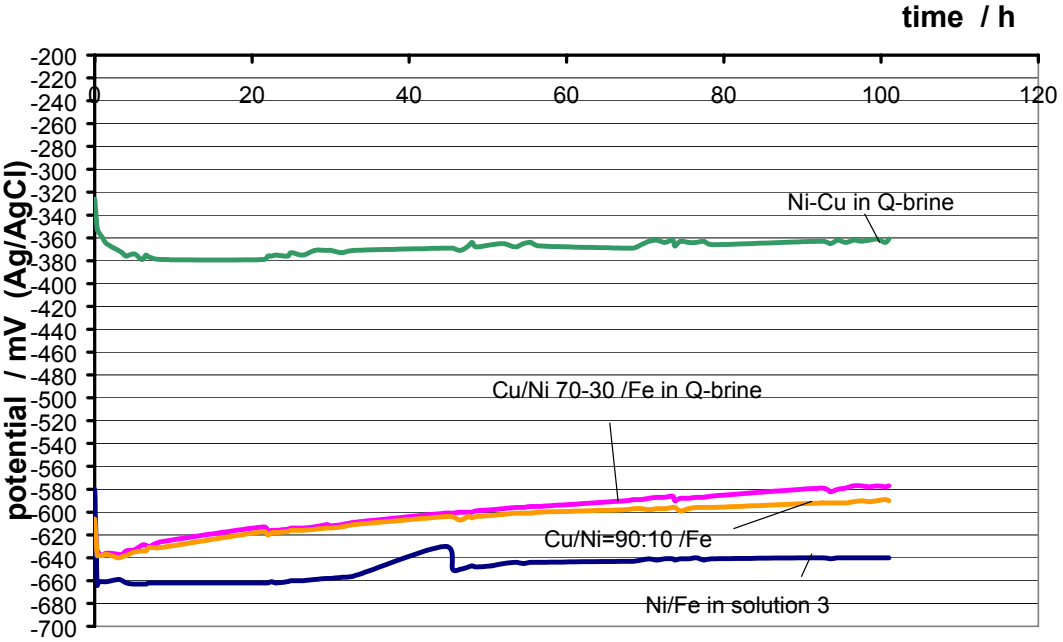

Figure 7: Contact potentials of the material pairs Ni/carbon steel, Ni/Cu and Cu-Ni alloys/carbon steel in brines at 80°C

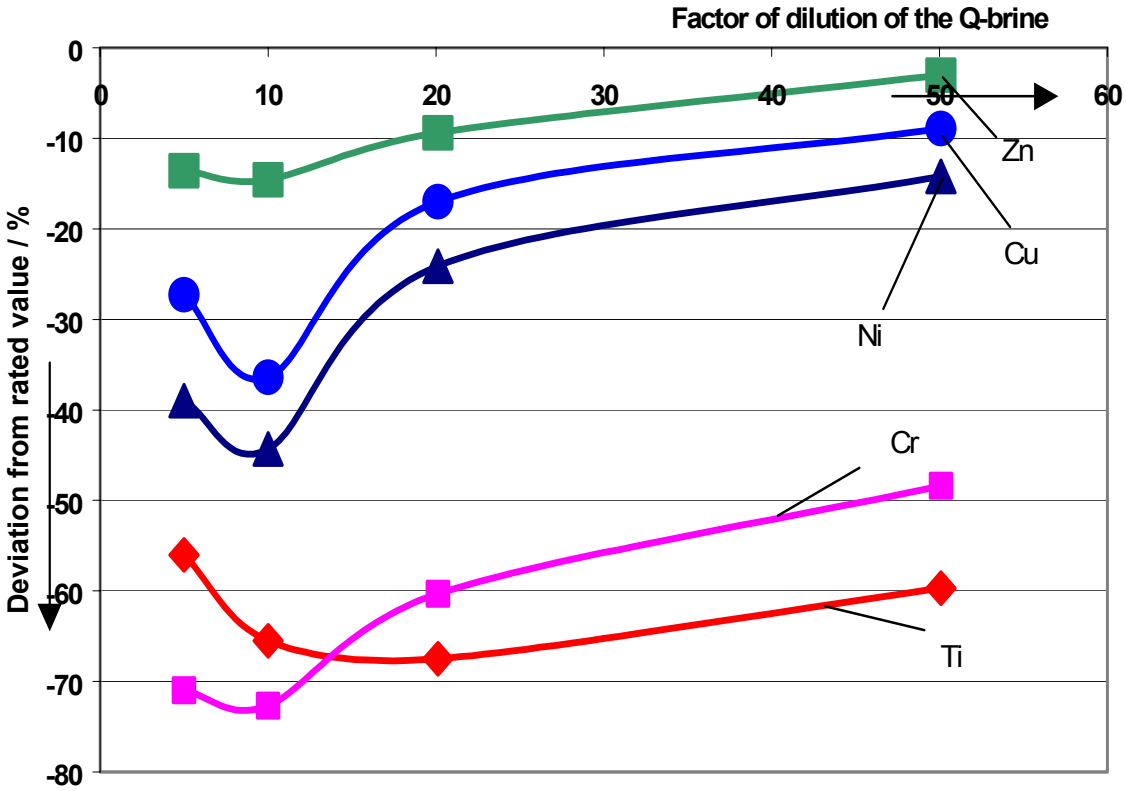

Figure 8: Influence of the dilution factor of the matrix Q-brine on the results of TXRL

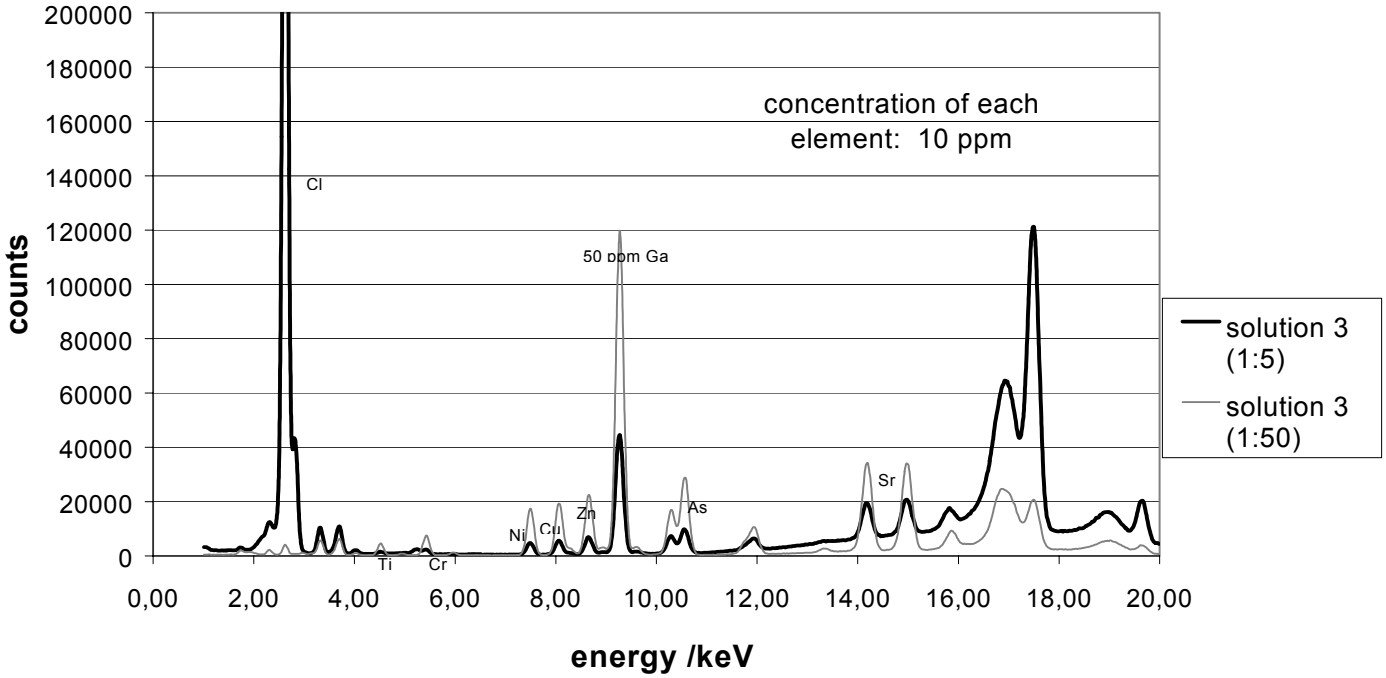

Figure 9: TXRF-spectra of a multielement standard in the NaCl-rich brine 3 at two different dilution factors

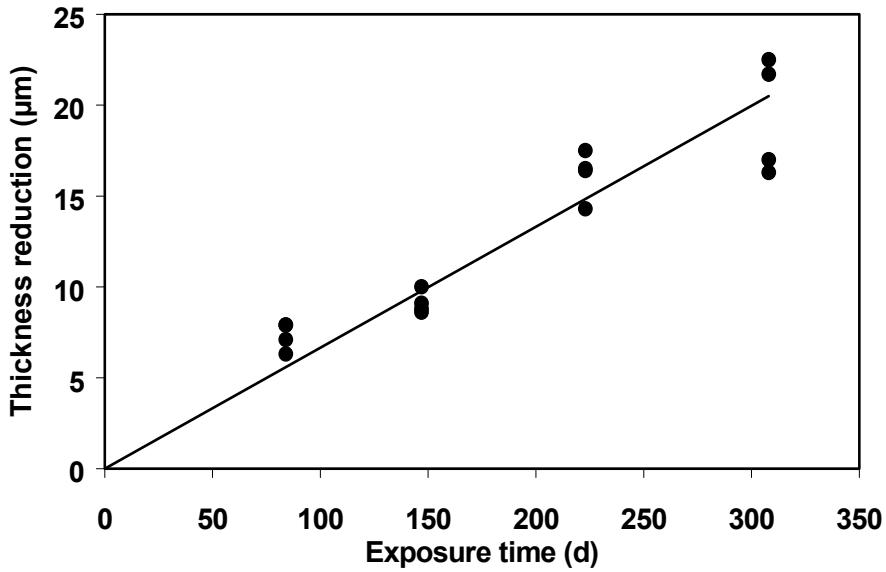

Figure 10: Time-dependence of the thickness reduction of the TStE 355 carbon steel in granitic water 1 at 90°C (98 mg/l Cl^-)

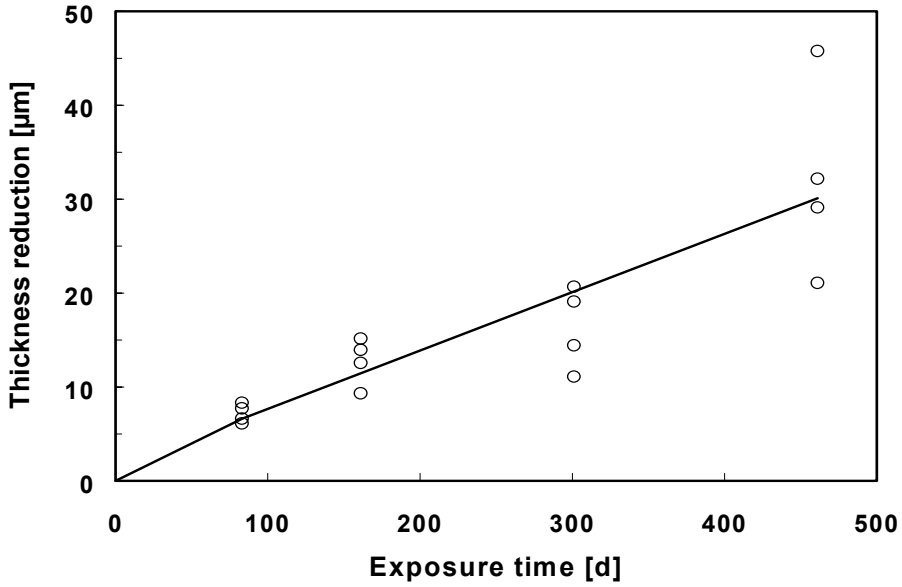

Figure 11: Time-dependence of the thickness reduction of the TStE355 carbon steel in granitic water 2 at 90°C (6260 mg/l Cl^-)

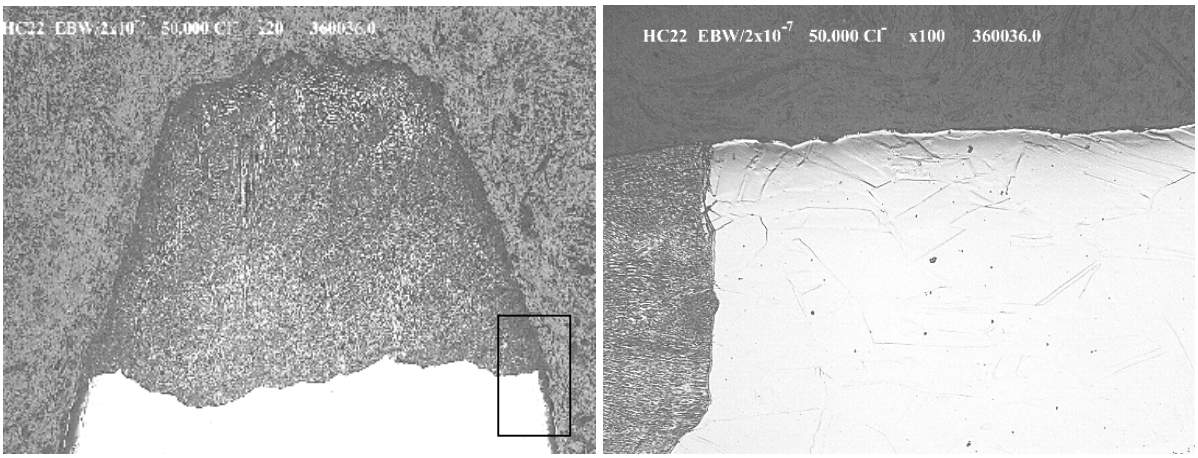

Figure 12: Optical micrographs of a SSR specimen of GTA welded HC-22 alloy tested at a strain rate of $2x10^{-7}s^{-1}$ in granitic water with a chloride content of 50000 ppm a) x15, b) x75.

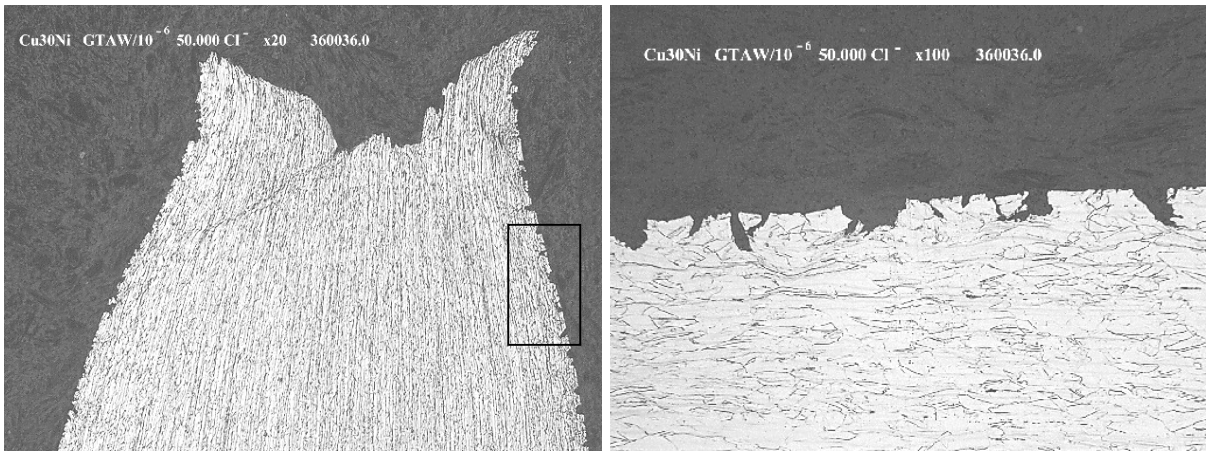

Figure 13: Optical micrographs of a SSR specimen of GTA welded Cu30Ni alloy tested at a strain rate of $10^{-6}s^{-1}$ in granitic water with a chloride content of 50000 ppm a) x15, b) x75.

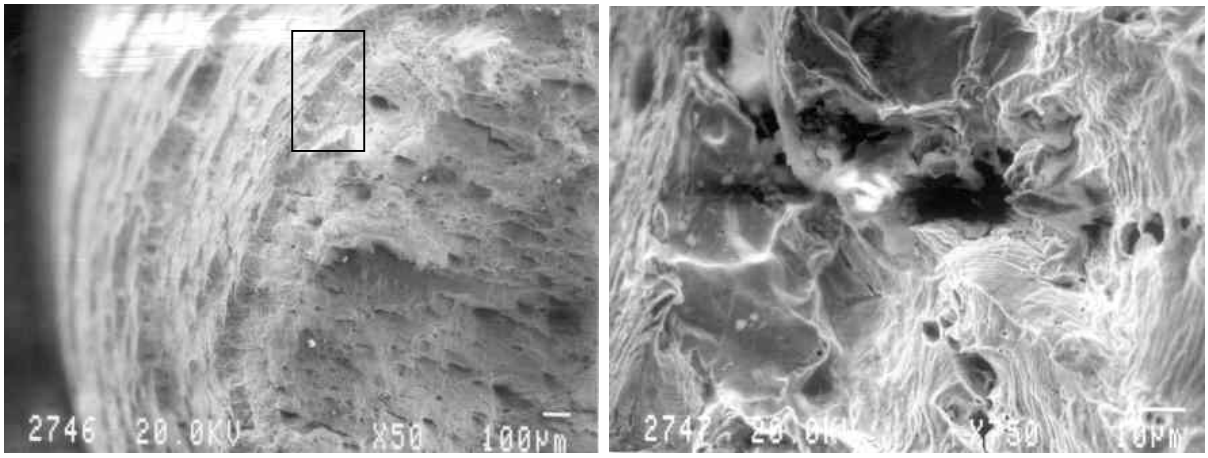

Figure 14: SEM micrographs of the fracture surface of a Cu30Ni alloy specimen tested at a strain rate of $2x10^{-7}s^{-1}$ in granitic water with a chloride content of 50000 ppm a) x50, b) x750.

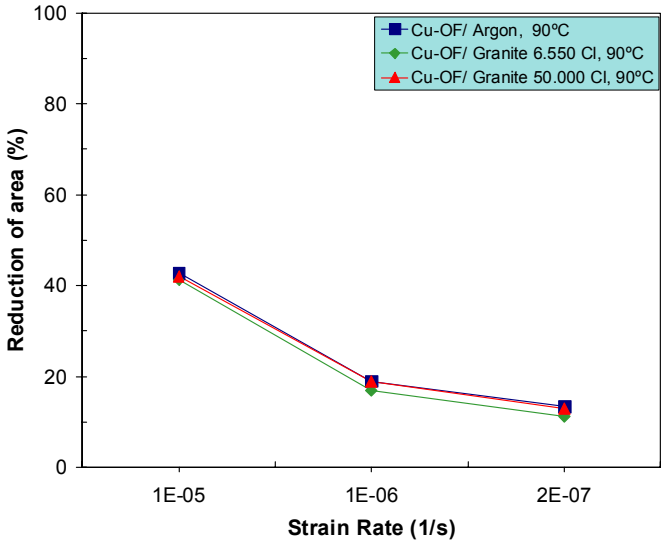

Figure 15: Reduction of area versus strain rate obtained for SSR Cu-OF specimens tested at 90ºC in argon and in granite with different chloride contents.

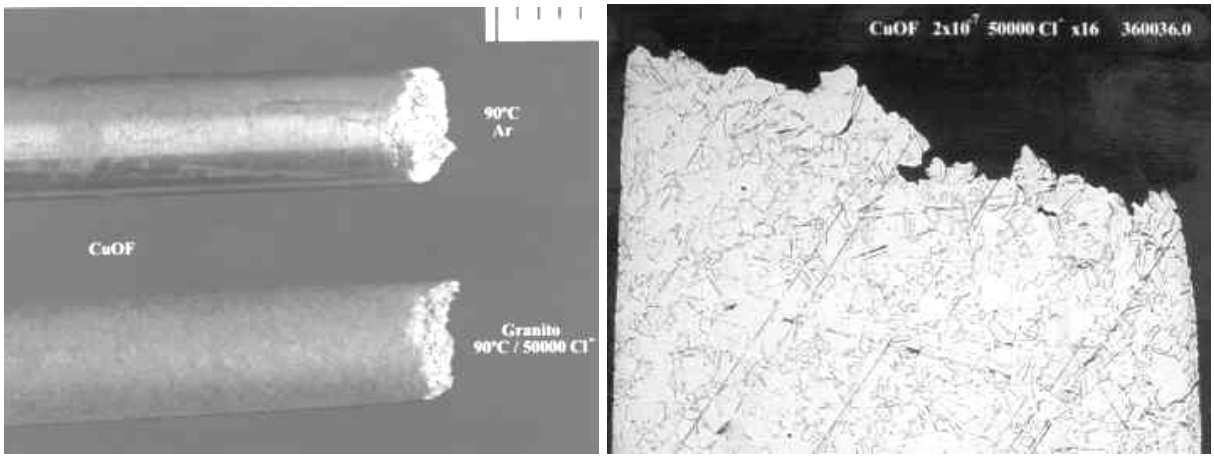

Figure 16: a) Macrograph showing SSR Cu-OF specimens tested at a strain rate of $2x10^{-7}s^{-1}$ in argon and in granitic water with 50000 ppm chloride, respectively ; b) Optical micrograph of the specimen tested in the granite-chloride water, x12.

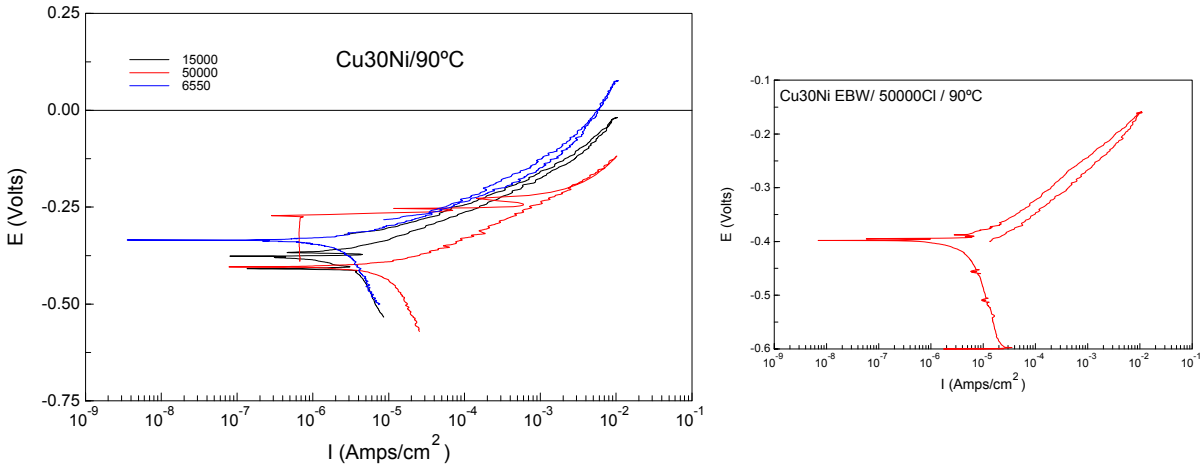

Figure 17: Polarization curves for Cu30Ni alloy tested at 90ºC in granitic water with different chloride contents.

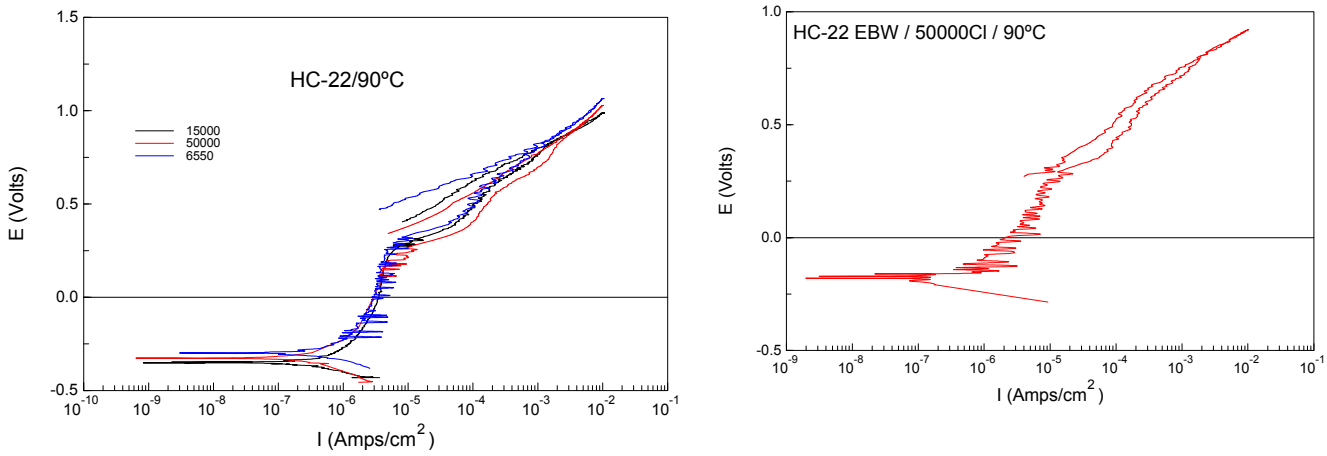

Figure 18: Polarization curves for Cu-OF alloy tested at 25ºC in granitic water with different chloride contents.

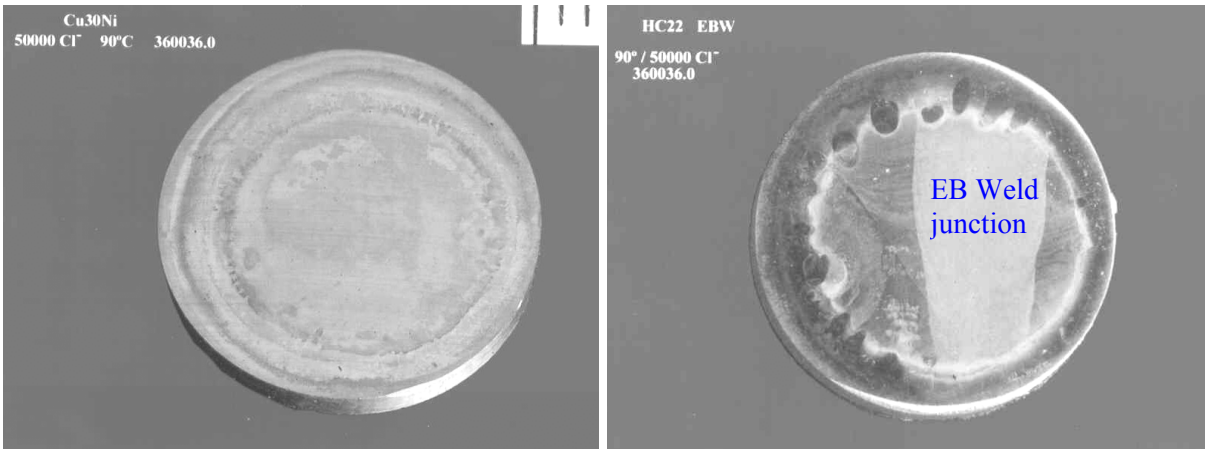

Figure 19: Surface appearance after potentyodinamic polarization test in granitic water at 90ºC and 50000 ppm chloride of a) Cu30Ni alloy specimen and b) HC-22 with EB welded joint. Specimen has been chemically etched.

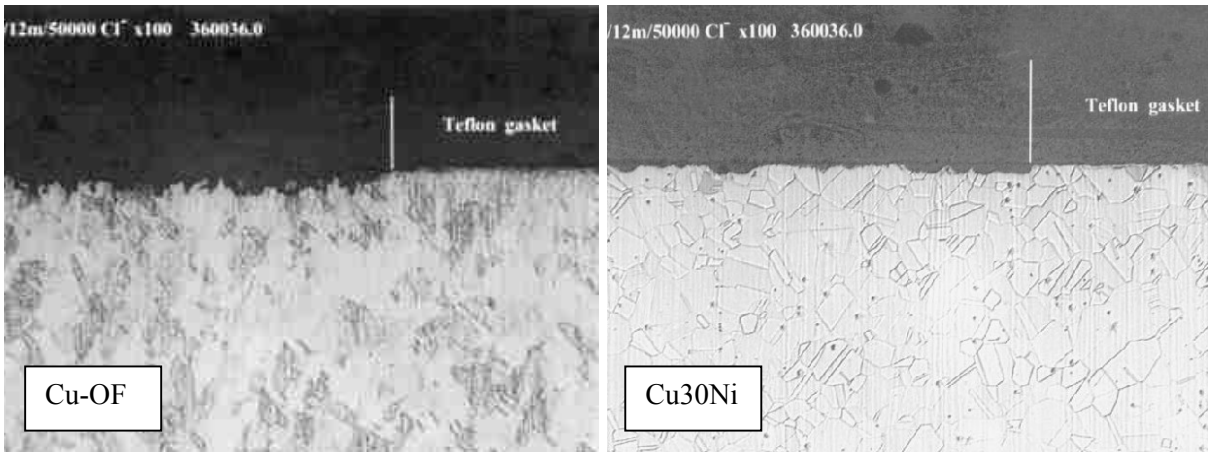

Figure 20: Optical micrographs of Cu-OF and Cu30Ni crevice specimens, after 12 months exposure to granitic water at 90ºC and a chloride content of 50000 ppm, x100.

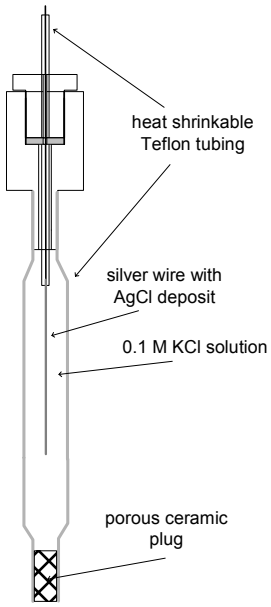

Figure 21**:** Schematic drawing of the internal Ag/AgCl reference electrode used to perform CPP-measurements at 140°C (autoclave experiments).

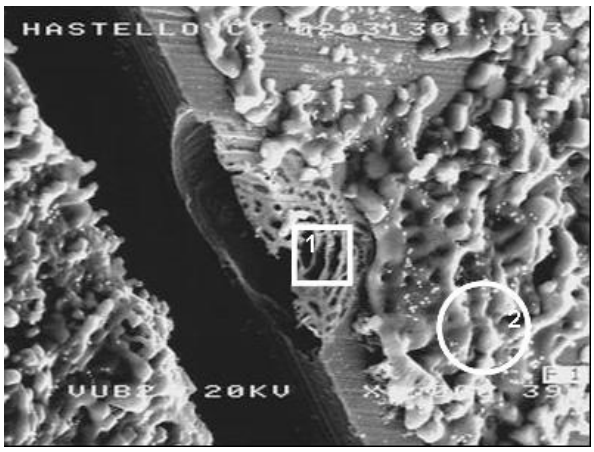

Fig.22: SEM-micrograph of an uncleaned HASTELLOY C-4 sample after CPP-testing in SOCW containing 216 mg/L SO_4^{2-} and 50,000 mg/L Cl^-.

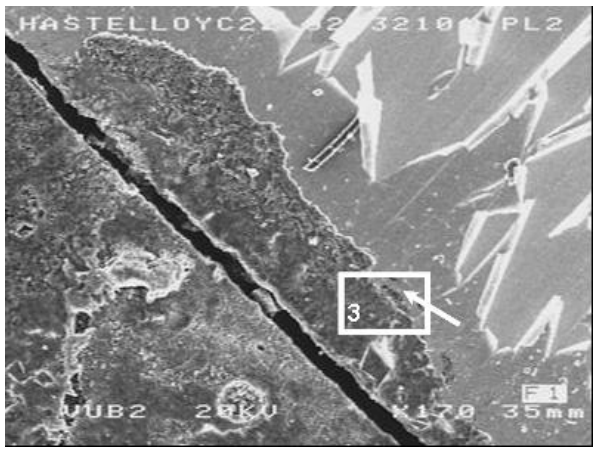

Fig.23**:** SEM-micrograph of an uncleaned HASTELLOY C-22 sample after CPP-testing in SOCW containing 216 mg/L SO_4^{2-} and 50,000 mg/L Cl^-.

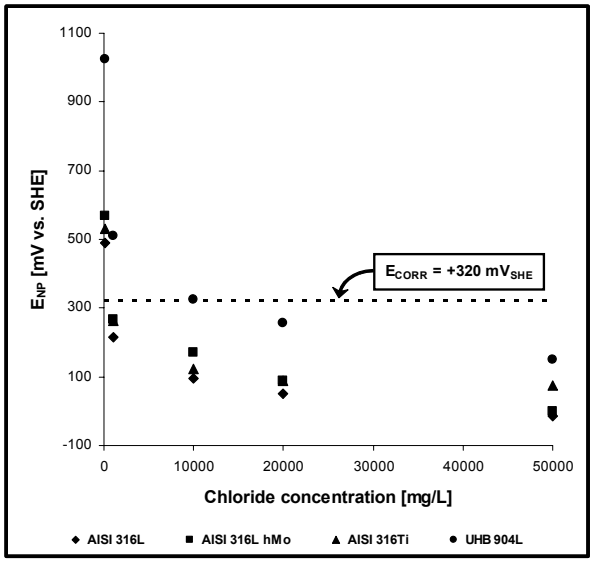

Fig.24: Influence of Cl^- on E_{NP} of 316L, 316L hMo, 316Ti, and UHB 904L stainless steel in SOCW containing 216 mg/L SO_4^{2-}.

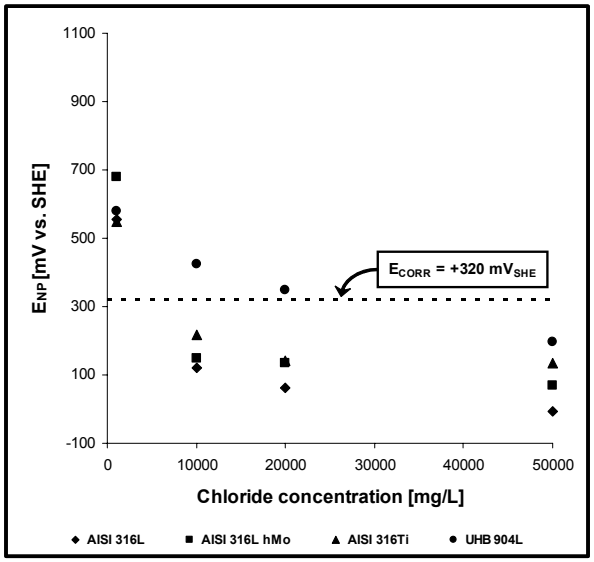

Fig.25: Influence of Cl^- on E_{NP} of 316L, 316L hMo, 316Ti, and UHB 904L stainless steels in SOCW containing 5.400 mg/L SO_4^{2-}.

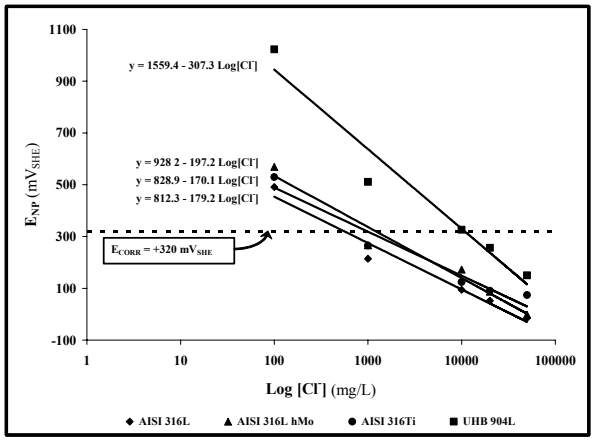

Fig.26: Linear fitting of (E_{NP}, log[Cl^-]) plots of 316L, 316L hMo, 316Ti,and UHB 904L stainless steels in SOCW containing 216 mg/L SO_4^{2-} *(140°C).*

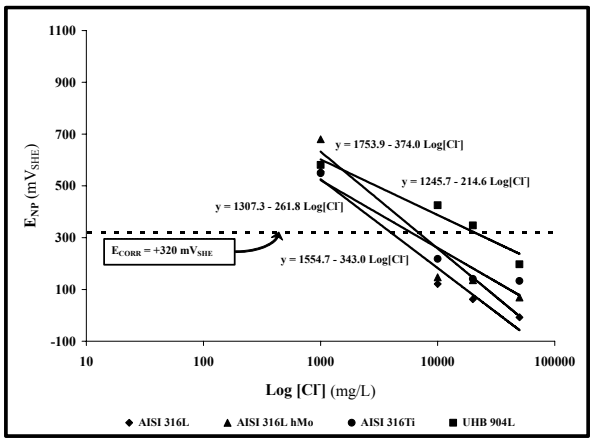

Fig.27: Linear fitting of (E_{NP}, log[Cl^-]) plots of 316L, 316L hMo, 316Ti, and UHB 904L stainless steels in SOCW containing 5,400 mg/L SO_4^{2-} (140°C)

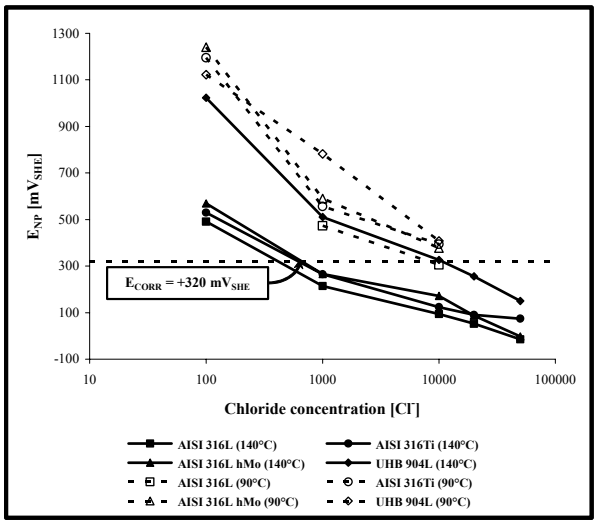

Fig.28: Influence of temperature on E_{NP} of 316L, 316L hMo, 316Ti, and UHB 904L stainless steel in SOCW containing 216 mg/L SO_4^{2-}.

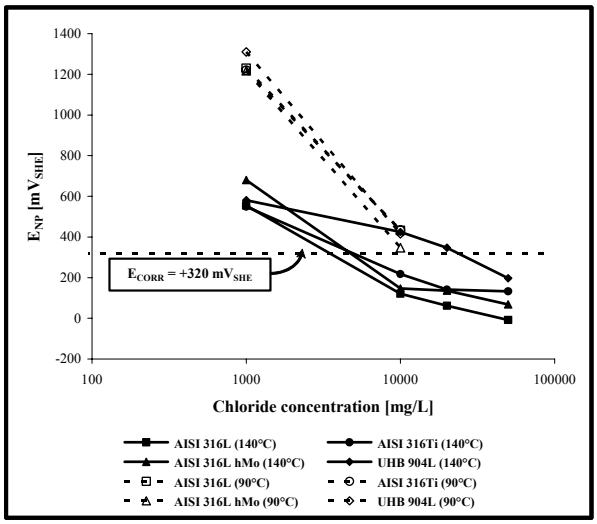

Fig.29: Influence of temperature on ENP of 316L, 316L hMo, 316Ti, and UHB 904L stainless steel in SOCW containing 5,400 mg/L SO_4^{2-}.

ANNEX: Updated Time Schedule (Project: Container Corrosion Studies)

State: October 2002

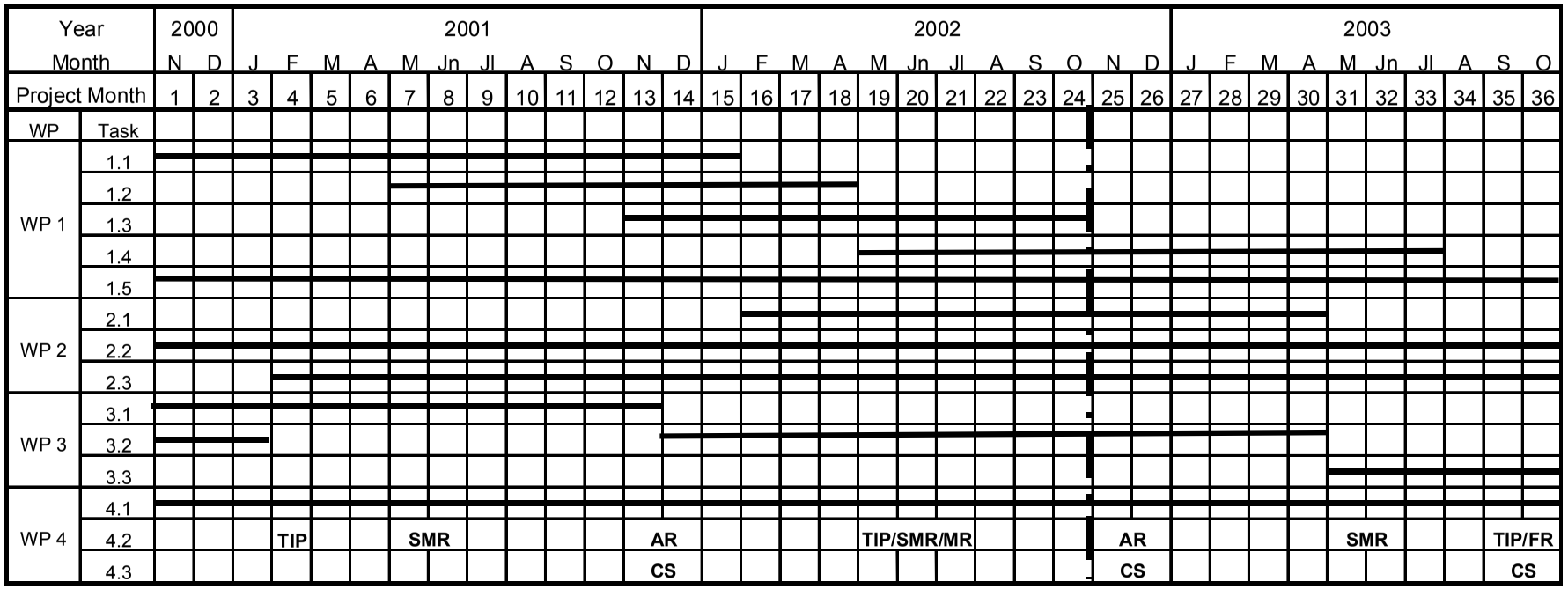

WP 1 : Salt environment
1.1 : Influence of thermal stress relief treatment on corrosion
1.2 : Contact corrosion between steel and Ti99.8-Pd
1.3 : Long-term corrosion studies on Cu-base materials
1.4 : Contact corrosion between steel and Cu-base materials
1.5 : Electrochemical corrosion studies

WP 2: Granitic environment
2.1 : Long-term corrosion studies on steel and Cu-base materials
2.2 : Stress corrosion cracking studies on Cu- and Ni-base materials
2.3 : Localized corrosion studies on Cu- and Ni-base materials

WP 3: Clay environment
3.1 : Influence of anaerobic conditions on corrosion
3.2 : Influence of elevated temperature on corrosion
3.3 : Influence of radiolysis products on corrosion

WP 4: Project management
4.1 : Co-ordination
4.2 : Reports
4.3 : Cost statements

TIP: Technolog. Implem. Plan
SMR: Six-months report
AR: Annual report
MR: Mid-term report
FR: Final report
CS: Cost statements

Time-Schedule-2.xls